A LAYERED MODEL APPROACH TO THE EARTH-IONOSPHERE CAVITY RESONANCE PROBLEM

by

WILLIAM B. THOMPSON

S. B., S. M., Massachusetts Institute of Technology

(1958)

SUBMITTED IN PARTIAL FULFILLMENT
OF THE REQUIREMENTS FOR THE
DEGREE OF DOCTOR OF
PHILOSOPHY

at the

MASSACHUSETTS INSTITUTE OF TECHNOLOGY

February, 1963

Signature of Author . . . . . .
Department of Geology and Geophysics
February 25, 1963

Certified by . . . . . .
Thesis Supervisor

Accepted by . . . . . .
Chairman, Departmental Committee
on Graduate Students

ABSTRACT

The purpose of this investigation is to define a satisfactory mathematical model to predict the character and propagation properties of the ELF resonant waves in the spherical cavity bound by the earth and ionosphere. The study of the modes of this cavity offers a useful geophysical tool for observation of the gross properties of the lower ionosphere, which comprises one wall of the cavity. The model uses real ionospheric parameters in the presence of the earth's geomagnetic field, which makes the conductivity anisotropic. The mode structure as observed at the earth's surface is affected by the conductivity of the ionosphere to varying heights.

A two-dimensional cylindrical model and a spherical model will be studied, the former to give some insight into the solutions for the latter, which is limited to the case of a radial geomagnetic field. Solutions to the wave equation for anisotropic media are found for a magnetic field aligned with any coordinate axis in the cylindrical model, and for a radial B field in the spherical model. Analytical solutions for several cases of elementary conductivity profiles are studied to evaluate qualitatively the affect of the geomagnetic field on the mode properties. The model is a layed profile with constant properties within each layer. This approach is valid due to the extremely long wavelengths involved.

Machine computations are used to solve the boundary-value problem of determining the resonant modes for models with varying numbers of layers ranging from three to sixty. Separate models treat the cases of longitudinal and transverse propagation in the cylindrical cavity, and a day and night ionosphere under longitudinal propagation for the spherical cavity. General results show higher peak frequencies for transverse than longitudinal propagation, and higher frequencies for the night than the day spherical problem. Investigations of the maximum altitude of the ionosphere effective in determining the resonant properties indicate that in the absence of a geomagnetic field cavity waves are confined to the region below 118 km., while the presence of a field of .4 Gauss allows some cavity energy to leak out into the region of free propagation above 200 km. Therefore, a large portion of the real ionosphere is effective in shaping the cavity response.

ACKNOWLEDGEMENTS

Initially let me express my thanks to my advisor, Prof. T. R. Madden, whose critical guidance throughout the course of this dissertation was of an invaluable nature. Many of the techniques used in the solution of the problem and the interpretation of results were used at his suggestion.

I am similarly indebted to Dr. M. Balser and Mr. C. A. Wagner of Lincoln Laboratory for many helpful discussions and suggestions.

Financial assistance to carry out this work was given by the M. I. T. Research Laboratory of Electronics and The American Chemical Society. Their support is gratefully acknowledged.

All numerical computations were done on the IBM 7090 at Lincoln Laboratory. Miss S. Sillers programmed the work. The manuscript was typed by Miss L. Giles.

TABLE OF CONTENTS

LIST OF FIGURES

LIST OF TABLES

CHAPTER I

INTRODUCTION, METHOD OF SOLUTION, AND THE CONDUCTIVITY TENSOR

1.1 Introduction

Recent experimental measurements [Balser and Wagner, 1960] have indicated that the spherical layer bounded by the earth and ionosphere acts as a resonant cavity to terrestrial ELF noise. Spectral analysis of noise received on a vertical whip antenna by Balser and Wagner in a 5-35 cps range gives the average peak frequencies of the first four modes of the cavity as 7.8, 14.1, 20.3, and 26.5 cps, respectively, with a Q ranging from 4 in the first mode to 6 in the higher ones. Theoretical work by Schumann [1952] had predicted the modes for a lossless cavity at frequencies of $f_n = 10.6 \sqrt{n(n+1)}/2$, where n is the order of the mode.

The problem of defining a satisfactory model to explain the observed phenomena has been a subject of recent interest. Models have been suggested, notably those of Galejs [1962], which have managed to duplicate the Balser and Wagner spectra in detail. However, no models to date have attempted to include the influence of the geomagnetic field, which makes the conducting ionosphere anisotropic.

The purpose of this thesis is to show that consideration of the geomagnetic field not only significantly modifies the mode properties of the isotropic model, but also extends the region which determines these properties to much greater altitudes. This purpose is accomplished by formulating a suitable mathematical model to describe the response of a cavity with appropriately real parameters to an electric dipole source. This is a satisfactory source, since Balser and Wagner [1961] have demonstrated that world-wide lightning storms act as the excitation for the real earth cavity.

Once the ability of the model to duplicate known experimental results is demonstrated, it may then be used to predict results of measurements not yet attempted. One of the features discussed is the altitude of penetration of energy at cavity frequencies in the ionosphere. The night ionosphere is most conducive to high altitude propagation, and a considerable portion of incident energy can penetrate well above 200 km. along a radial geomagnetic field. Removal of the geomagnetic field in the model confines

cavity waves to below 120 km. at night, and below 100 km. in the day. Existence of cavity waves at high altitudes exhibits the feasibility of measuring the cavity spectrum from satellites, possibly on a foreign planet.

The character of the resonant modes necessarily reflects the integrated propagation properties of the entire cavity. Therefore this is a useful geophysical tool for studying the gross structure of the lower ionosphere. Local anomalies in propagation properties covering small areas relative to the whole cavity will of course be undetected. The difference in response between a cavity with a typical noon ionosphere and one with a typical night ionosphere, both with a radial geomagnetic field throughout, is only about one cycle in the first mode and three cycles in the fourth mode. On the basis of this, high altitude nuclear detonations of large yield might possibly be detectable as a perturbation of the normal cavity response. Solar events which cause such disturbances as a significant charge density increase in the D layer offer a similar possibility.

The mode structure of models of the earth-ionosphere cavity will be analyzed both in a cylindrical and a spherical system. Unfortunately in the spherical problem only the case of a radial geomagnetic field has a solution expressible in terms of known functions, making it the only case amenable to machine computation. This is the case of longitudinal propagation, since the index of refraction in the ionosphere is so much greater than in air that waves incident on the ionosphere at any angle propagate essentially in the radial direction. Examination of the quasi-longitudinal and quasi-transverse approximations of magneto-ionic theory for plane waves indicates that at cavity frequencies propagation is nearly longitudinal everywhere except in a narrow region around the geomagnetic equator. This is strictly valid when the conductivity depends only on electrons, which will be shown to correspond to the region below 100 km. The increasing importance of ions above 100 km., however, should effect only minor changes in this description. It should be remarked that even though longitudinal propagation is correct for most of the cavity, the propagation constant still changes with geomagnetic latitude. The model cannot handle parameter changes in other than the radial direction, so that radial symmetry is used throughout.

Thesis Outline

Chapter I includes introductory remarks and a derivation of the general conductivity tensor appropriate to the ionosphere below 400 km.

Chapter II contains the derivation of the wave solutions for anisotropic media necessary to solve the boundary-value problem.

Chapter III presents the analytical solutions to several elementary models and points out the affect of the magnetic field's magnitude and direction on the cavity response.

Chapter IV discusses the conductivity of the ionosphere up to several hundred kilometers and describes the role of the ions in the day (noon) and night (midnight) models.

Chapter V gives the numerical results concerning peak frequencies and Q's of models with large numbers of layers, and conclusions as to the role of the geomagnetic field in determining these properties.

1.2 Method of Solution

The boundary-value problem of finding the mode structure of the cavity will be solved in two different coordinate systems. It will first be done in a two-dimensional cylindrical system, and then in the more appropriate spherical coordinate system. Solutions in cylindrical coordinates can be obtained for a geomagnetic field directed along either of the three coordinate axes while the spherical system only allows simple solutions for a radially oriented field. Solutions for a radial geomagnetic field are shown to be very similar in the two geometries when the model is elementary.

The cavity may be thought of as consisting of three zones; namely the earth, the air layer, and the ionosphere. The earth's surface will be treated as a perfect reflector at these low frequencies. The air layer will have the propagation properties of free space. And the properties of the ionosphere will be represented by a tensor conductivity which varies only in the radial direction.

At ELF reflection properties change considerably over one wavelength. For such low frequency waves the ionosphere can be represented by a series of concentric spherical shells, each shell having constant conductivity properties in itself, with a shell thickness much less than a wavelength.

The source in the model is a vertical electric dipole located in the air layer close to the earth. This is the best analog to the actual lightning source.

It is clear from the above description that parameter changes in other than the radial direction are not accounted for in this model. This excludes the difference in day and night ion density profiles, and also tensor conductivity changes as a function of geomagnetic latitude. However an attempt will be made to place limits on the real mode properties by solving the problem in the various extreme cases.

Preliminary model results indicated that the ionosphere above 100 km. must be considered in determining cavity properties. At these heights the effect of ions on the conductivity components must be considered.

Once the wave solutions for anisotropic media have been determined, the mechanics of actually setting up the problem for machine computation will be handled in matrix form as described by Madden [1961].

1.3 The Conductivity Tensor

Following Akasofu [1956] the equations of motion of a ternary mixture of electrons, positive ions and neutral particles in the presence of a magnetic field are given by:

$$\rho_n \frac{\partial \vec{v}_n}{\partial t} + N_n N_p \alpha_{en} (\vec{v}_n - \vec{v}_e) + N_n N_p \alpha_{in} (\vec{v}_n - \vec{v}_i) = 0 \qquad 1.3.1$$

$$\rho_e \frac{\partial \vec{v}_e}{\partial t} + N_p^2 \alpha_{ie} (\vec{v}_e - \vec{v}_i) + N_n N_p \alpha_{en} (\vec{v}_e - \vec{v}_n) = -e N_p (\vec{E} + \vec{v_e \times B}) \qquad 1.3.2$$

$$\rho_i \frac{\partial \vec{v}_i}{\partial t} + N_p^2 \alpha_{ie} (\vec{v}_i - \vec{v}_e) + N_n N_p \alpha_{in} (\vec{v}_i - \vec{v}_n) = e N_p (\vec{E} + \vec{v_i \times B}) \qquad 1.3.3$$

The pressure terms have been neglected and we assume $\frac{\partial v_i}{\partial t} \gg v \cdot \text{grad } v_i$ (subscript i refers to direction)

$$\alpha_{ij} = \nu_{ij} \frac{m_i m_j}{\rho_i + \rho_j}$$

The subscript e = electrons, i = ions, and n = neutrals.

The plasma is electrically neutral, so $N_i = N_e = N_p$.

ρ = mass density of particles ($\rho_n = m_n N_n$, etc.)

v = velocity varying as exp ($-i\omega t$)

$m = m_i + m_e$

N = particles cm^{-3}.

B = geomagnetic Field Strength.

ν_{ij} = average collision frequency between particles of type i and j.

Define a plasma current as $J = e (N_i v_i - N_e v_e)$.

The solution of (1.3.1 - 1.3.3) gives a vector equation of the form $E_i = R_{ij} J_j$, where R_{ij} is the tensor resistivity. Leaving the details of the solution and the approximations involved to Appendix I, the resulting equation is:

$$\vec{E} = \vec{J}\frac{m_e}{e^2 N_p}(\nu_{ie} + \nu_{en} - i\omega) + \frac{\vec{J}\times\vec{B}}{e N_p} - \frac{(\vec{J}\times\vec{B})\times\vec{B}}{m N_p(\nu_{in} - i\omega)} \qquad 1.3.4$$

Let

$$x = \frac{m_e}{e^2 N_p}(\nu_{ie} + \nu_{en} - i\omega)$$

$$y = \frac{1}{N_p e}$$

$$z = 1/m N_p (\nu_{in} - i\omega)$$

The boundary value problem is manageable only when the geomagnetic field is along one of the coordinate axes. Therefore the conductivity tensor must be evaluated for three separate cases. When dealing in spherical coordinates these cases are $B_0 = B_r$, $B_0 = B_\theta$, and $B_0 = B_\phi$.

Case I. $B_0 = B_r$, $B_\theta = B_\phi = 0$

$$R_{ij} = \begin{vmatrix} x & 0 & 0 \\ 0 & x + B_0^2 z & yB_0 \\ 0 & -yB_0 & x + B_0^2 z \end{vmatrix} \qquad 1.3.5$$

The conductivity tensor $\sigma_{ij} = R_{ij}^{-1}$.

$$\sigma_{ij} = \begin{vmatrix} \frac{1}{x} & 0 & 0 \\ 0 & \frac{x+B_0^2 z}{(x+B_0^2 z)^2+y^2 B_0^2} & \frac{-y B_0}{(x+B_0^2 z)^2+y^2 B_0^2} \\ 0 & \frac{y B_0}{(x+B_0^2 z)^2+y^2 B_0^2} & \frac{x+B_0^2 z}{(x+B_0^2 z)^2+y^2 B_0^2} \end{vmatrix} \qquad 1.3.6$$

Defining the three different conductivity terms as follows,

$$\sigma_{11} = \frac{Ne^2}{m_e} \frac{1}{(\nu_e - i\omega)} \qquad 1.3.7$$

where $N_p = N$,

$\nu_e = \nu_{ei} + \nu_{en}$

and $\nu_{ei} = \nu_{ie}$

$$\sigma_\perp = Ne^2 \left[\frac{\nu_e - i\omega}{m_e [(\nu_e - i\omega)^2 + \omega_H^2]} + \frac{\nu_i - i\omega}{m_i [(\nu_i - i\omega)^2 + \Omega_H^2]} \right] \qquad 1.3.8$$

$$\sigma_x = Ne^2 \left[\frac{\Omega_H}{m_i [(\nu_i - i\omega)^2 + \Omega_H^2]} - \frac{\omega_H}{m_e [(\nu_e - i\omega)^2 + \omega_H^2]} \right] \qquad 1.3.9$$

$$\text{then } \sigma_{ij} = \begin{vmatrix} \hat{r} & \hat{\theta} & \hat{\phi} \\ \sigma_{11} & 0 & 0 \\ 0 & \sigma_\perp & \sigma_x \\ 0 & -\sigma_x & \sigma_\perp \end{vmatrix} \qquad 1.3.10$$

Case II, $B_0 = B_\theta$, $B_r = B_\phi = 0$

$$R_{ij} = \begin{vmatrix} x+B_0^2 z & 0 & -y B_0 \\ 0 & x & 0 \\ y B_0 & 0 & x+B_0^2 z \end{vmatrix} \qquad 1.3.11$$

$$\sigma_{ij} = \begin{vmatrix} \sigma_\perp & 0 & -\sigma_x \\ 0 & \sigma_{11} & 0 \\ \sigma_x & 0 & \sigma_\perp \end{vmatrix} \qquad 1.3.12$$

Case III $B_0 = B_\phi$, $B_r = B_\theta = 0$

$$R_{ij} = \begin{vmatrix} x+B_0^2 z & yB_0 & 0 \\ -yB_0 & x+B_0^2 z & 0 \\ 0 & 0 & x \end{vmatrix} \qquad 1.3.13$$

$$\sigma_{ij} = \begin{vmatrix} \sigma_\perp & \sigma_x & 0 \\ -\sigma_x & \sigma_\perp & 0 \\ 0 & 0 & \sigma_{11} \end{vmatrix} \qquad 1.3.14$$

There are regions in the D layer where negative ions are present in greater density than either electrons or positive ions. However, in Sections (5.2-4) it will be shown that they are not dense enough to make more than a one per cent change in the conductivity computed on the assumption that $N_e = N_i^+$.

CHAPTER II

THE WAVE SOLUTIONS FOR ANISOTROPIC MEDIA

2.1 The Cylindrical Problem

Before the cavity resonance problem can be attacked, the wave solutions for electromagnetic propagation in anisotropic media must be derived. Section 1.3 demonstrates that the geomagnetic field makes the medium anisotropic. When $B_0 = 0$, $\sigma_x = 0$, $\sigma_\perp = \sigma_{11}$, so the conductivity tensor reduces to a scalar quantity.

The geomagnetic field is considered in one coordinate direction at a time. The problem is two-dimensional in that $\frac{\partial}{\partial z} = 0$. The time dependence of the solution is $\exp(-i\omega t)$ and the angular dependence is $\exp(in\theta)$. The θ dependence is $\exp(in\theta)$ in the air and must be the same in the ionosphere if boundary conditions are to be satisfied at the air-ionosphere interface.

The geometry of the problem is given in Figure 1.

Fig. 1

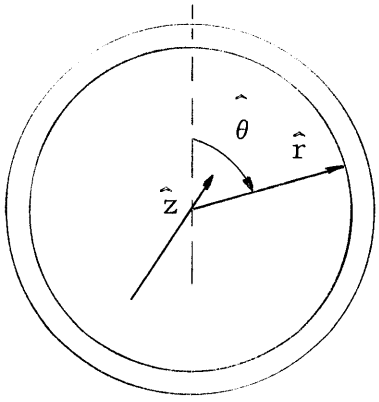

The two Maxwell equations expressing the wave properties are

$$(\text{curl } E)_i = -\frac{\partial B_i}{\partial t} = +i\mu\omega H_i \qquad 2.1.1$$

$$(\text{curl } H)_i = \sigma_{ij} E_j + \frac{\partial D_i}{\partial t} \qquad 2.1.2$$

Displacement currents will be neglected in the ionosphere.

The wave solutions are found by solving (2.1.1) and (2.1.2) using the σ_{ij} of Section 1.3 appropriate to the geomagnetic field to direction. For a magnetic field in the $\hat{z}$ direction these solutions are given in Appendix II-A. This is the only example of anisotropy where the two waves present can be distinguished as a TE and TM mode similar to the isotropic waves. TE waves are described by $H_n(k_p r)$ and $\frac{\partial H_n(k_p r)}{\partial r}$ functions where $k_p^2 = k_\perp^2 + \frac{k_x^4}{k_\perp^2}$. We define $k_{11}^2 = i\mu\omega\sigma_{11}$, $k_\perp^2 = i\mu\omega\sigma_\perp$, and $k_x^2 = i\mu\omega\sigma_x$. This mode is clearly affected by the magnetic field, since both $k_\perp$ and k_x depend on B_0. This is expected, since the TE mode has E_r and E_θ components, both of which move electrons transverse to the B field.

The TM mode propagates independent of the geomagnetic field with $k = k_{11}$ as though the medium were isotropic; its only E vector is E_z, and therefore it ignores the magnetic field. The propagation constants for these two modes are just those which describe the plane wave case of transverse propagation.

When the geomagnetic field is in the θ direction the TE-TM mode description breaks down. There are still two distinct waves, but each wave now has E and H components in all three directions. One wave again propagates as a k_p mode, but when $B_0 \to 0$, this becomes the isotropic TM mode. The other wave propagates as k_{11} and when $B_0 \to 0$ reduces to the isotropic TE mode. For the case $B_z = B_0$, it was the k_p wave which described the TE mode and the k_{11} wave which described the TM mode. When $B_0 \to 0$, of course, $k_p = k_{11}$.

The two waves present in this case ($B_\theta = B_0$) have quite different properties in addition to their propagation constants. For the k_p wave, E_z is a factor of (kr) larger than E_θ, while the opposite is true for the k_{11} wave. Similarly H_θ is a factor of (kr) larger than H_z for the k_p wave, and H_z is (kr) greater than H_θ in the k_{11} wave.

This case of $B_\theta = B_0$ may be thought of as transverse propagation; indeed, k_p and k_{11} are the plane wave transverse constants. But the k_{11} wave cannot ignore the magnetic field as when $B_z = B_0$. B_0 has coupled the Maxwell equations so that each field component is related to every other one; therefore the solutions for the k_{11} wave necessarily depend on B_0.

When the geomagnetic field is in the radial direction each of the two modes present again involves all six field components. The propagation constant is the same as that for longitudinal propagation in the plane wave case; i.e. $k^2 = k_\perp^2 \pm ik_x^2$.

This summarizes the results of the wave solutions in this system when the geomagnetic field is along any one of the coordinate axes. Although one would similarly expect the propagation constant for a magnetic field at an arbitrary angle to be the same as in the plane wave case (which is known), the boundary value problem cannot be approached until the wave solutions in the ionosphere are known in a form compatible with the solutions in the air. Such solutions may be obtainable in two dimensions, but have no hope in the spherical system, as will be seen shortly.

2.2 The Spherical Problem

Although this is the most appropriate geometry in which to solve the cavity problem for the earth, the mathematics limits one to the case of longitudinal propagation; i.e. radial propagation and a radial geomagnetic field. The restricting influence is due to the angular dependent terms in the Maxwell equations.

Longitudinal $\hat{\phi}$ dependence is eliminated by placing the dipole source at $\theta = 0$. In order to match boundary conditions at the air-ionosphere interface it is expected that the same Legendre polynomials will describe the θ (latitude) dependence in both zones, thus leaving the solution for the radial dependence of thefield vectors as the only unknown. The usual $\hat{\theta}$ dependence in air is

$$E_r,\ H_r = P_n(\cos\theta)\, E_r(r),\ \text{etc.}$$

$$E_\theta,\ H_\theta, E_\phi,\ H_\phi = \frac{dP_n(\cos\theta)}{d\theta}\, E_\theta(r),\ \text{etc.} \qquad 2.2.1$$

The following table summarizes the latitude dependence for the known isotropic case and shows how the Maxwell equations are modified by the geomagnetic field.

Maxwell Equation	Isotropic Solution Common Factor	New Terms Introduced due to Anisotropy		
		B_r	B_θ	B_ϕ
$(\text{curl } H)_r$	P_n	0	$dP_n/d\theta$	$dP_n/d\theta$
$(\text{curl } H)_\theta$	$dP_n/d\theta$	$dP_n/d\theta$	0	P_n
$(\text{curl } H)_\phi$	$dP_n/d\theta$	$dP_n/d\theta$	P_n	0
$(\text{curl } E)_r$	P_n	0	0	0
$(\text{curl } E)_\theta$	$dP_n/d\theta$	0	0	0
$(\text{curl } E)_\phi$	$dP_n/d\theta$	0	0	0

Only the column of terms under B_r (longitudinal propagation) introduce the Legendre polynomial such that it can still be factored out of the component equation, as in the isotropic case. The other two B_0 field orientations would introduce a $dP_n/d\theta$ term into an equation where all other terms are P_n, and vice versa; i.e. the assumed latitude dependence is incorrect and the true dependence is unknown. We are therefore limited to the case of a radial B field where only the radial dependence of the field components must be solved for.

The wave solutions for longitudinal propagation described in Appendix II-D have the same propagation constant as the radial case in cylindrical coordinates. The only approximation made in obtaining these solutions is that $k_\perp^2 r^2$ and $k_{11}^2 r^2 \gg n(n+1)$. This places a lower bound on the electron density in any layer at about $10/cm^3$. This means that in practice the model ionosphere profile begins at 50 km. for the noon case and 80 km. for the night case. The skin depth for such a density is on the order of 1000 km. for cavity frequencies, so the less dense regions below these bounds have little influence on ELF propagation.

The wave solutions (D.2.4) of Appendix II indicate that the polarization of the longitudinal wave is circular.

Top sign $\qquad E_\phi = i E_\theta$

$\qquad H_\phi = i H_\theta$

Bottom sign $\qquad E_\phi = -i E_\theta$

$\qquad H_\phi = -i H_\theta$

and, for either sign, $\frac{E_\phi}{E_\theta} = -\frac{H_\theta}{H_\phi}$.

CHAPTER III

THE ANALYTICAL SOLUTION FOR THE RESONANT MODES OF SEVERAL ELEMENTARY MODELS

3.1 General

Before the results of the problem done for an extremely large number of layers are discussed, it is of interest to examine the analytical solution for some very simple conductivity profiles. Indeed, once the problem is set up for a one-layer ionosphere, the extension to n-layers is straightforward so far as machine computation is concerned.

3.2 The Layer Geometry

Fig. 2

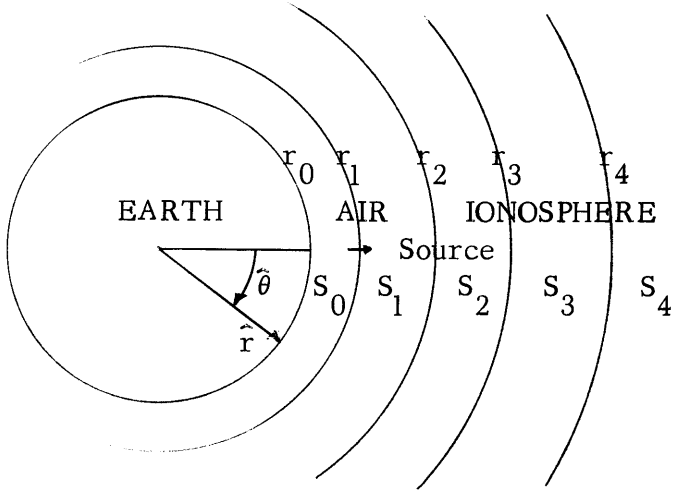

Figure 2 represents the geometry of the problem. The conductivity at r_o, the mean radius of the earth, is taken to be infinite. The source is a vertical electric dipole in spherical coordinates located at the boundary layer r_1. The source position is taken as $\theta = 0$; therefore there is no ϕ (longitude) dependence in the solutions. In cylindrical coordinates the source is an infinite line of similar dipoles extending in the $\hat{z}$ direction. Hence in either system the coordinates $\hat{r}$ and $\hat{\theta}$ adequately describe the geometry. The electromagnetic field of this dipole (or array) is such that it directly excites the TE mode in the air. If the TE mode can exist in the ionosphere (anisotropic medium), then this will be the only mode necessary to describe the solutions. Such is

the case for $B_z = B_0$ in the cylindrical system. If, however, all field vectors are coupled to one another, as is the case for $B_\theta = B_0$ and $B_r = B_0$, then there must be a TM mode in the air in order to satisfy the boundary conditions at $r = r_2$.

3.3 The Matrix Solution of the Boundary-Value Problem

A matrix form of solution applicable to problems of this nature is described by Madden [1961]. Let

$$S_n(r) = a_n(r)\, c_n \qquad 3.3.1$$

in the n^{th} layer, where S_n is a column matrix of the field vectors which enter into the boundary conditions, a_n is the solution matrix and c_n is the coefficient matrix. S_n is valid at both r_n and r_{n+1}, so (3.3.1) may be written

$$S_n(r_{n+1}) = a_n(r_{n+1})\, c_n$$

$$S_n(r_n) = a_n(r_n)\, c_n \qquad 3.3.2$$

Solving (3.3.2) to eliminate c_n,

$$S_n(r_n) = a_n(r_n)\, a_n^{-1}(r_{n+1})\, S_n(r_{n+1}) \qquad 3.3.3$$

The boundary condition at $r = r_1$, $\theta = 0$ is

$$S_0(r_1) = S_1(r_1) + Q(\text{source}) \qquad 3.3.4$$

and at all other r_n it is

$$S_n(r_{n+1}) = S_{n+1}(r_{n+1}) \qquad 3.3.5$$

Combining 3.3.3-5 the vectors at the earth's surface, $S_0(r_0)$, can be expressed in terms of the vectors at the outermost boundary

$$S_0(r_0) = a_0(r_0)\, a_0^{-1}(r_1)\, Q + a_0(r_0)\, a_0^{-1}(r_1)\, a_1(r_1) \text{ ---}$$

$$\text{--- } a_n(r_n)\, a_n^{-1}(r_{n+1})\, S_n(r_{n+1}) \qquad 3.3.6$$

3.4 An Infinitely Conducting Ionosphere in Cylindrical Coordinates

This problem is confined to the air layer and is, of course, isotropic. Only the components E_θ and H_z of the TE mode are necessary to describe the problem.

$$S_0(r_0) = \begin{vmatrix} E_\theta(r_0) \\ H_z(r_0) \end{vmatrix}, \qquad Q = \begin{vmatrix} 1 \\ 0 \end{vmatrix}$$

$$a_0(r) = a_1(r) = \begin{vmatrix} -i\mu\omega \dfrac{\partial H_n^{(1)}}{\partial r}(k_0 r) & -i\mu\omega \dfrac{\partial H_n^{(2)}}{\partial r}(k_0 r) \\ k_0^2 H_n^{(1)}(k_0 r) & k_0^2 H_n^{(2)}(k_0 r) \end{vmatrix}$$

where the n subscript of $H_n(k_0 r)$ indicates the order of the mode and is not related to the layer number. Equation (3.3.6) becomes

$$S_0(r_0) = a_0(r_0)\, a_0^{-1}(r_1)\, Q + a_0(r_0)\, a_0^{-1}(r_1)\, a_1(r_1)\, a_1^{-1}(r_2)\, S_1(r_2) \qquad 3.4.1$$

Let $r_0 = a$ = radius of the earth

$r_1 \cong r_0 = a$, so $a_0(r_0)\, a_0^{-1}(r_1) = I$ (unit matrix)

also $a_0^{-1}(r_1)\, a_1(r_1) = I$, since $a_0 = a_1$

$$S_1(r_2) = \begin{vmatrix} E_\theta(r_2) \\ H_z(r_2) \end{vmatrix}$$

Since the boundary at a and r_2 is perfectly reflecting, Equation (3.4.1) becomes

$$\begin{vmatrix} 0 \\ H_z(r_0) \end{vmatrix} = a_0(r_0)\, a_1^{-1}(r_2) \begin{vmatrix} 0 \\ H_z(r_2) \end{vmatrix} + \begin{vmatrix} 1 \\ 0 \end{vmatrix} \qquad 3.4.2$$

Let $r_2 = a + h$, where $h \ll a$. At ELF $h \ll \lambda$ and a Taylor expansion is used to express Hankel functions at $r_0 = a$ in terms of those at r_2. λ is the wavelength.

$$H_n(k_0 a) = H_n(k_0 r_2)\left(1 + \frac{nh}{r_2}\right) - k_0 h\, H_{n-1}(k_0 r_2) \qquad 3.4.3$$

Using the approximation (3.4.3) and the fact that $h \ll a$,

$$a_0(r_0)\, a_1^{-1}(r_2) = \begin{vmatrix} 1 & -i\mu\omega h\left(1 - \frac{n^2}{k_0^2 r_2^2}\right) \\ -\frac{ik_0^2 h}{\mu\omega} & 1 \end{vmatrix}$$

Substituting (3.4.4) into (3.4.2) and solving for $H_z(r_0) = \dfrac{1}{i\mu\omega h\left(1 - \frac{n^2}{k_0^2 r_2^2}\right)}$ 3.4.5

$H_z(r_0) \to \infty$ when $k_0^2 r_2^2 = n^2$ or at

$$f_n = \frac{1}{2\pi}\,\frac{cn}{r_2} \qquad 3.4.6$$

where f_n is the frequency in cps, and c is the speed of light in free space.

Since both cavity walls are perfect reflectors and the air medium is lossless, the Q of the cavity is infinite.

The frequency of the n^{th} mode in the equivalent spherical geometry as given by Schumann is $f_n = \frac{1}{2\pi}\,\frac{c}{a}\sqrt{n(n+1)}$.

3.5 A One-Layer Ionosphere of Infinite Extent in Cylindrical Coordinates; Radial Geomagnetic Field

In this case we extend Equation(3.4.1) by

$$S_1(r_2) = S_2(r_2) = a_2(r_2)\, c_2 \qquad 3.5.1$$

The anisotropy of the ionosphere layer forces consideration of all components of E and H in order to satisfy the boundary conditions at r_2

$$S_0(r_0) \begin{vmatrix} E_\theta(r_0) \\ H_z(r_0) \\ E_z(r_0) \\ H_\theta(r_0) \end{vmatrix}, \quad Q = \begin{vmatrix} 1 \\ 0 \\ 0 \\ 0 \end{vmatrix}, \quad c_2 = \begin{vmatrix} A \\ 0 \\ B \\ 0 \end{vmatrix}$$

where the zeros in c_2 are the coefficients of the return wave in the ionosphere.

The expression for the mode problem becomes

$$\begin{vmatrix} 0 \\ H_z(r_0) \\ 0 \\ H_\theta(r_0) \end{vmatrix} = a_0(r_0)\, a_1^{-1}(r_2)\, a_2(r_2) \begin{vmatrix} A \\ 0 \\ B \\ 0 \end{vmatrix} + \begin{vmatrix} 1 \\ 0 \\ 0 \\ 0 \end{vmatrix} \qquad 3.5.2$$

where

$$a_0(r) = a_1(r) = \begin{vmatrix} -i\mu\omega \frac{\partial H_n^{(1)}}{\partial r}(k_0 r) & -i\mu\omega \frac{\partial H_n^{(2)}}{\partial r}(k_0 r) & 0 & 0 \\ k_0^2 H_n^{(1)}(k_0 r) & k_0^2 H_n^{(2)}(k_0 r) & 0 & 0 \\ 0 & 0 & k_0^2 H_n^{(1)}(k_0 r) & k_0^2 H_n^{(2)}(k_0 r) \\ 0 & 0 & \frac{ik_0^2}{\mu\omega} \frac{\partial H_n^{(1)}}{\partial r}(k_0 r) & \frac{ik_0^2}{\mu\omega} \frac{\partial H_n^{(2)}}{\partial r}(k_0 r) \end{vmatrix} \qquad 3.5.3$$

and, from Appendix II, Equations C.2.4 with $k_2^2 = k_\perp^2 + ik_x^2$ and $k_3^2 = k_\perp^2 - ik_x^2$,

$$a_2(r) = \begin{vmatrix} \frac{-ie^{ik_2 r}}{\sqrt{r}} & \frac{-ie^{-ik_2 r}}{\sqrt{r}} & \frac{ie^{ik_3 r}}{\sqrt{r}} & \frac{ie^{-ik_3 r}}{\sqrt{r}} \\ \frac{-e^{ik_2 r}}{\mu\omega\sqrt{r}}(ik_2 + \frac{1}{2r}) & \frac{-e^{-ik_2 r}}{\mu\omega\sqrt{r}}(-ik_2 + \frac{1}{2r}) & \frac{e^{ik_3 r}}{\mu\omega\sqrt{r}}(ik_3 + \frac{1}{2r}) & \frac{e^{-ik_3 r}}{\mu\omega\sqrt{r}}(-ik_3 + \frac{1}{2r}) \\ \frac{e^{ik_2 r}}{\sqrt{r}} & \frac{e^{-ik_2 r}}{\sqrt{r}} & \frac{e^{ik_3 r}}{\sqrt{r}} & \frac{e^{-ik_3 r}}{\sqrt{r}} \\ \frac{ie^{ik_2 r}}{\mu\omega\sqrt{r}}(ik_2 - \frac{1}{2r}) & \frac{ie^{-ik_2 r}}{\mu\omega\sqrt{r}}(-ik_2 - \frac{1}{2r}) & \frac{ie^{ik_3 r}}{\mu\omega\sqrt{r}}(ik_3 - \frac{1}{2r}) & \frac{ie^{-ik_3 r}}{\mu\omega\sqrt{r}}(-ik_3 - \frac{1}{2r}) \end{vmatrix}$$

3.5.4

From (3.5.3) in conjunction with (3.4.3) it can be shown that

$$a_0(r_0)\, a_1^{-1}(r_2) = \begin{vmatrix} 0 & -i\mu\omega h(1 - \frac{n^2}{k_0^2 r_2^2}) & 0 & 0 \\ \frac{-ik_0^2 h}{\mu\omega} & 1 & 0 & 0 \\ 0 & 0 & 1 & i\mu\omega h \\ 0 & 0 & \frac{ihk_0^2}{\mu\omega}(1 - \frac{n^2}{k_0^2 r_2^2}) & 1 \end{vmatrix}$$

3.5.5

Substituting (3.5.4) and (3.5.5) into (3.5.2) and solving for $H_z(r_0)$,

$$-i\mu\omega\, H_z(a) = \frac{(k_0^2 h + ik_2 + \frac{1}{2r_2})(1 - ihk_3) + (k_0^2 h + ik_3 + \frac{1}{2r_2})(1-ihk_2)}{\left[1 - h(1 - \frac{n^2}{k_0^2 r_2^2})(ik_3 + \frac{1}{2r_2})\right](1-ihk_2) + \left[1-h(1-\frac{n^2}{k_0^2 r_2^2})(ik_2+\frac{1}{2r_2})\right](1-ihk_3)}$$

3.5.6

where k_0 is the free space propagation constant

and $h = r_2 - r_0$ = thickness of the air layer.

The presence of k_2 and k_3 in the denominator of (3.5.6) makes it complex; therefore the cavity has a finite Q. The two variables in $H_z(a)$ are n, the mode order, and the frequency f, which is implied in the k's. The structure of the first mode is realized by plotting for n = 1, the magnitude of $H_z(a)$ as a function of f.

3.6 One Layer Ionosphere of Infinite Extent in Cylindrical Coordinates; Geomagnetic Field in $\hat{z}$ Direction

This is the one orientation of geomagnetic field for which the two distinct TE and TM modes exist in the ionosphere. Since the source excites only the TE mode in the air, this is the only mode necessary to describe the problem.

The solution to the resonance problem is found by solving for $H_z(r_0)$ in

$$\begin{vmatrix} 0 \\ H_z(r_0) \end{vmatrix} = a_0(r_0)\, a_1^{-1}(r_2)\, a_2(r_2) \begin{vmatrix} A \\ 0 \end{vmatrix} + \begin{vmatrix} 1 \\ 0 \end{vmatrix} \qquad 3.6.1$$

where $a_0(r_0)\, a_1^{-1}(r_2)$ is given by (4.4.4) and from (2.2.5) and (2.2.7)

$$a_2(r) = \begin{vmatrix} \dfrac{i\sigma_x \frac{n}{r} H_n^{(1)}(k_p r) - \sigma_\perp \frac{\partial H_n^{(1)}}{\partial r}(k_p r)}{\sigma_\perp^2 + \sigma_x^2} & \dfrac{i\sigma_x \frac{n}{r} H_n^{(2)}(k_p r) - \sigma_\perp \frac{\partial H_n^{(2)}}{\partial r}(k_p r)}{\sigma_\perp^2 + \sigma_x^2} \\ H_n^{(1)}(k_p r) & H_n^{(2)}(k_p r) \end{vmatrix}$$

3.6.2

where $k_p^2 = k_\perp^2 + k_x^4/k_\perp^2$

The solution of (3.6.1) is

$$i\mu\omega H_z(a) = \frac{k_0^2 h\left[-i\sigma_x \frac{n}{r_2} H_n^{(1)}(k_p r_2) + \sigma_\perp \frac{\partial H_n^{(1)}}{\partial r}(k_p r_2)\right] - i\mu\omega H_n^{(1)}(k_p r_2)(\sigma_\perp^2 + \sigma_x^2)}{i\sigma_x \frac{n}{r_2} H_n^{(1)}(k_p r_2) - \sigma_\perp \frac{\partial H_n^{(1)}}{\partial r_2}(k_p r_2) - i\mu\omega h\left(1 - \frac{n^2}{k_0^2 r_2^2}\right) H_n^{(1)}(k_p r_2)(\sigma_\perp^2 + \sigma_x^2)} \qquad 3.6.3$$

Using the exponential approximation to the Hänkel function for $k_p r_2 \to \infty$, Equation (3.6.3) reduces in the isotropic case to

$$-i\mu\omega H_z(a) = \frac{ik_0^2 h - k_{11}}{i + k_{11} h\left(1 - \frac{n^2}{k_0^2 r_2^2}\right)} \qquad 3.6.4$$

for $k_{11} r \gg 1$.

This is obtained by letting $k_p \to k_{11}$, $\sigma_\perp \to \sigma_{11}$ and $\sigma_x \to 0$.

A comparison of Equations (3.5.6) and (3.6.3) indicates the difference in the resonance expression for a very simple geometry when the direction of the geomagnetic field differs by 90°. Equation (3.6.3) can be compared with its isotropic reduction (3.6.4) to show that the anisotropic problem has a solution equivalent to that for an isotropic ionosphere with conductivity equal to $\sigma = \sigma_\perp + \frac{\sigma_x^2}{\sigma_\perp}$.

Since, in (3.6.3), $k_p r_2 \gg 1$, we can write

$$\frac{\partial H_n}{\partial r_2}(k_p r_2) = H_n(k_p r_2)\, ik_p \qquad 3.6.5$$

A valid approximation is that $\frac{\sigma_x}{r_2} \ll \sigma_\perp k_p$. This can be demonstrated by squaring both sides

$$\sigma_x^2 \ll r_2^2 \sigma_\perp^2 k_p^2 = r_2^2 \sigma_\perp^2 \left(k_\perp^2 + \frac{k_x^4}{k_\perp^2}\right)$$

$$= \sigma_\perp^2 k_\perp^2 r_2^2 + \sigma_x^2 k_\perp^2 r_2^2 \qquad 3.6.6$$

and in the model it is always true that $k_\perp^2 r^2 \gg 1$.

Using (3.6.5) and (3.6.6) for small n (we shall only discuss the first few modes of the cavity) reduces expression (3.6.3) to

$$-i\mu\omega H_z(a) = \frac{i k_0^2 h - k_p}{i + h k_p (1 - \frac{n^2}{k_0^2 r_2^2})} \qquad 3.6.7$$

Expression (3.6.7) compares directly with (3.6.4) if one substitutes $k_{11} = k_p$ into the isotropic result. It should be remarked here that in the special case that only the electrons are considered in the conductivity tensor, an identity exists relating the components as follows:

$$\sigma_{11}\sigma_\perp = \sigma_\perp^2 + \sigma_x^2 \qquad 3.6.8$$

Whenever (3.6.8) is true, it can readily be shown that $k_p = k_{11}$ even when the geomagnetic field is present. It will be pointed out in Chapter 4 that the ions have little affect on the conductivity below 100 km. Therefore in this region (3.6.8) is approximately true and both the isotropic and anisotropic waves propagate with the same velocity, although their wave solutions remain different.

Under isotropic conditions of k_2, $k_3 \rightarrow k_{11}$, expression (3.5.6) reduces to (3.6.4) just as (3.6.3) did. This is expected, since the magnetic field direction was the only difference in the two problems to which (3.5.6) and (3.6.3) are solutions.

The resonance expression (3.5.6) for a radial B field is equivalent to the isotropic case (3.6.4) with $\sigma_{11} = 2\sigma_x$ whenever $k_x \gg k_\perp$ and $k_x h \gg 1$. This means that, at least in the simple one layer geometry, an ionosphere with a radial B field resonates as an isotropic one with conductivity $\sigma = 2\sigma_x$, and an ionosphere with an axial B field resonates as an isotropic one with conductivity $\sigma = \sigma_p$.

3.7 One Layer Ionosphere of Finite Extent in Cylindrical Coordinates; Radial Geomagnetic Field

This is the next step of complication after the one infinite layer ionosphere. The solution to the resonance problem is expressed by

$$\begin{vmatrix} 0 \\ H_z(r_0) \\ 0 \\ H_\theta(r_0) \end{vmatrix} = a_0(r_0)a_1^{-1}(r_2)a_2(r_2)a_2^{-1}(r_3) \begin{vmatrix} 0 \\ H_z(r_3) \\ 0 \\ H_\theta(r_3) \end{vmatrix} + \begin{vmatrix} 1 \\ 0 \\ 0 \\ 0 \end{vmatrix} \qquad 3.7.1$$

where $a_0(r_0)\, a_1^{-1}(r_2)$ is given by (3.5.5) and $a_2(r_2)$ is given by (3.5.4). Because of the two zeros in the vector column at r_3, only the second and fourth column terms of $a_2(r_2)\, a_2^{-1}(r_3)$ are required. Solution of (3.7.1) for $H_z(r_0)$ is

$$H_z(r_0) = \frac{AA^* - BB^*}{CC^* - DD^*} \qquad 3.7.2$$

where

$$t_1 = \frac{\sinh(ik_2h_1)}{ik_2}, \quad t_2 = \frac{\sinh(ik_3h_1)}{ik_3}, \quad t_3 = \cosh(ik_2h_1), \quad t_4 = \cosh(ik_3h_1)$$

$$k_2^2 = k_\perp^2 + ik_x^2, \quad k_3^2 = k_\perp^2 - ik_x^2$$

a = radius of earth

h = height of air layer

h_1 = thickness of ionosphere

$R_1 = a + h$

$q = 1 - n^2/k_0^2 R_1^2$

and

$$A = -(t_1 + t_2)/4R_1 + (t_3 + t_4)/2$$

$$A^* = \frac{i\mu\omega}{2}\left[(t_1 + t_2) + h(t_3 + t_4)\right]$$

$$B = i(t_2 - t_1)/4R_1 + i(t_3 - t_4)/2$$

$$B^* = \frac{\mu\omega}{2}\left[(t_1 - t_2) + h(t_3 - t_4)\right]$$

$$C = \frac{\mu\omega}{2}\left[(t_1 - t_2)\left(1 - \frac{hq}{2R_1}\right) + hq\,(t_3 - t_4)\right]$$

$$C^* = \frac{\mu\omega}{2}\left[(t_1 - t_2) + h(t_3 - t_4)\right]$$

$$D = \frac{-i\mu\omega}{2}\left[(t_1 + t_2)\left(1 - \frac{hq}{2R_1}\right) + hq\,(t_3 + t_4)\right]$$

$$D^* = \frac{i\mu\omega}{2}\left[(t_1 + t_2) + h(t_3 + t_4)\right]$$

In the isotropic case for $k_2 = k_3 = k_{11}$ (3.7.2) reduces to

$$i\mu\omega\ H_z(r_0) = \frac{ik_{11} - \frac{1}{2R_1}\tanh(i\,k_{11}\,h_1)}{\tanh(i\,k_{11}h_1) + ik_{11}h\left(1 - \frac{n^2}{k_0^2 R_1^2}\right)} \qquad 3.7.3$$

Comparison of (3.7.2) and (3.7.3) gives an indication of the complexity introduced into the problem by the presence of the magnetic field. The actual numerical solution of (3.7.2) for the peak frequencies and Q's of the modes is too difficult to attempt by hand and will be postponed to Chapter 5 when the machine computations will be discussed. Suffice it to say at this time that hand computations of mode properties have been carried out by Madden [1961] for isotropic spherical problems of a single infinite layer and single finite layer ionosphere. Numerical results of these two problems achieved a close fit to the measured properties given by Balser and Wagner, at the expense of using unrealistic conductivities.

Numerical solution for the simple geometries derived in this section would be no more than an exercise. The problem of interest will be to study the magnetic field effects on the mode structure in a realistic model whose conductivity profile for a large number of layers closely approximates the real case.

3.8 One Layer Ionosphere of Infinite Extent in Spherical Coordinates; Radial Geomagnetic Field

Since the spherical problem will comprise the main body of the numerical results, only one analytical solution will be presented. The matrix solution to this problem is given by

$$\begin{vmatrix} E_\theta(r_0) \\ H_\phi(r_0) \\ E_\phi(r_0) \\ H_\theta(r_0) \end{vmatrix} = \begin{vmatrix} 0 \\ H_\phi(a) \\ 0 \\ H_\theta(a) \end{vmatrix} = a_0(a)\, a_1^{-1}(r_2)\, a_2(r_2) \begin{vmatrix} A \\ 0 \\ B \\ 0 \end{vmatrix} + \begin{vmatrix} 1 \\ 0 \\ 0 \\ 0 \end{vmatrix} \qquad 3.8.1$$

where $a_0(a)\, a_1^{-1}(r_2)$ and $a_2(r_2)$ are given in Appendix III as (A.3.3) and (A.3.4), respectively. The solution to (3.8.1) is

$$H_\phi(a) = \frac{N^*}{D^*} \quad \text{where} \qquad 3.8.2$$

$$N^* = (\sigma_0 h i k_1 - \sigma_\perp - i\sigma_x)(k_3 + \mu\omega h [\sigma_\perp - i\sigma_x])$$

$$+ (\sigma_0 h i k_3 - \sigma_\perp + i\sigma_x)(k_1 + \mu\omega h [\sigma_\perp + i\sigma_x])$$

$$D^* = (i k_3 + \frac{hP}{\sigma_0 a^2} [\sigma_\perp - i\sigma_x])(-k_1 - \mu\omega h [\sigma_\perp + i\sigma_x])$$

$$+ (i k_1 + \frac{hP}{\sigma_0 a^2} [\sigma_\perp + i\sigma_x])(-k_3 - \mu\omega h [\sigma_\perp - i\sigma_x])$$

where $P = k_0^2 a^2 - n(n+1)$.

In the isotropic case $k_1 = k_3 = k_{11}$ and $\sigma_x = 0$. In this case (3.8.2) becomes

$$-i\mu\omega\, H_\phi(a) = \frac{-k_{11} + i k_0^2 h}{i + k_{11} h [1 - \frac{n(n+1)}{k_0^2 a^2}]} \qquad 3.8.3$$

Comparing (3.8.3) with the appropriate cylindrical solution (3.6.4) points out the similarity in the response of the two resonant cavities. Since $r_2 \cong a$, the only real difference is that the n^2 in the two-dimensional system is $n(n+1)$ in the spherical system. The choice of r_2 or a merely depends on which direction the Taylor expansion goes; i.e. whether $H_n(kr_2)$ is expressed in terms of $H_n(ka)$, or vice versa.

Furthermore, the anisotropic solutions (3.8.2) and (3.5.6) are also identical save for the factor containing the n's, when $k_2, k_3 \gg \frac{1}{r_2}$. Unfortunately, no comparison can be made of solutions under anything but a radial B field, but it does seem likely that the differences in mode structure due to different orientations of the B field in cylindrical coordinates will give an indication of the differences to be expected if all cases could be done in the spherical system.

CHAPTER IV

THE CONDUCTIVE PROPERTIES OF THE IONOSPHERE

4.1 General

Before the actual model results are presented, a discussion of the conductive properties of the ionosphere to be used in the model is necessary. Since these properties are known to vary with time of day, solar activity, and geomagnetic latitude, the conditions under which the model data are valid must be established. Local noon and midnight profiles will be used for typical quiet solar periods at mid latitudes.

The possibility of a resonance occurring in the ion conductivity should be considered in the event that any of the cavity energy propagates to an altitude of 250 km or greater. It is feasible that proper conditions in the anisotropic media will allow a relatively undamped mode to reach this zone.

4.2 The Ion Composition of the Noon Ionosphere

Of the various data including charged particle density, collision frequency, and geomagnetic field strength essential to the calculation of the conductivity, perhaps the most inconclusive at this time is the ion composition, especially below 100 km. Nicolet and Aikin [1960] conclude that in the region 60-65 km the important ions are N_2^+, O_2^+, and O_2^-. This is the region where the ratio of negative ions to electrons is significant, being 7.5 at 60 km, .63 at 70 km, and becoming negligible at increased altitudes. Above 75 km one can assume that the positive ion density is equal to the electron density. Ionization in the 60-65 km region is due to cosmic ray effects. All three ions present to any abundance have concentrations greater than that of electrons with O_2^- being most dense. Mitra has pointed out that O_2^- and O^- are the only two stable negative ions in the ionosphere.

From 65-70 km Lyman alpha ionization of nitric oxide produces enough NO^+ ions to make them significant. Rather than a direct production, it is also likely that a reaction of O^+ with molecular nitrogen is responsible for the NO^+.

Above 70 km NO^+ becomes more dominant and remains so for the rest of the D layer.

Above 85 km X-ray produced ionization of O_2^+ and N_2^+ is significant enough to make the O_2^+ density comparable with that of NO^+. There is some question as to which of these two components is more important in this part of the E region which extends to about 150 km. The Wallops Island data [Taylor and Brinton, 1961] seems to favor an initial abundance of NO^+, with about equal densities of NO^+ and O_2^+ at 140 km. The Arctic data [Johnson, Meadows, and Holmes, 1958] favors an initial abundance of O_2^+, but was taken under conditions of polar blackout, as compared with normal conditions for the Wallops Island data. The calculations of Sagalyn, Smiddy, and Wisnia [1963] indicate a 3/2 ratio of NO^+/O_2^+ at 150 km.

At about 150 km the O^+ ion appears and gradually takes precedent so that it represents 80% of the positive ion concentration at 200 km, and better than 95% of the total ion concentration from 250-350 km.

It should be pointed out that electron and ion concentrations in the D layer can increase by factors of 10 to 100 during solar disturbances. The charged particle concentration is also known to increase with increasing geomagnetic latitude in the D layer, changing by as much as a factor of 3 compared with its equatorial value.

4.3 Analysis of Table I and Figure 3

Table I presents data indicating the influence of the ions on the conductivity at various altitudes for a noon ionosphere. The fourth and fifth columns give the order of magnitude of the affect of the ions on the tensor conductivity components. The computation is made assuming that the density of the underlined ion equals the electron density. The single deviation is at 180 km where the two underlined ions each have a density equal to half that of electrons.

In the 60 km region where negative ions are important (the total ion density is as great as 15 times that of electrons) the table shows that an ion density (and therefore conductivity) two orders of magnitude greater than that of electrons would make only a 1% change in $\sigma_\perp$ and virtually none in σ_x. The same is true at 70 km where ions are less than 10 times as dense as electrons.

TABLE I

Phase of Propagation Vectors when f = 13.5 cps

Noon Ionosphere, B = .4 Gauss

Longitudional Propagation

Altitude	Important Ions	$\left\lvert \sigma_x/\sigma_\perp \right\rvert$	$\left\lvert \frac{[\sigma_x]\ \text{ion}}{[\sigma_x]\ \text{el}} \right\rvert$	$\left\lvert \frac{[\sigma_\perp]\ \text{ion}}{[\sigma_\perp]\ \text{el}} \right\rvert$	θ_3	θ_1
60 km	$0_2^+, N_2^+, 0_2^-$	10^{-1}	10^{-8}	10^{-4}	65^o	35^o
70 km	$0_2^+, N_2^+, 0_2^-, N_0^+$	1	10^{-7}	10^{-3}	72^o	18^o
80 km	NO^+	10	10^{-6}	10^{-2}	86^o	4^o
90 km	$NO^+, 0_2^+$	10	10^{-4}	1	89^o	1^o
100 km	$NO^+, 0_2^+$	10	10^{-2}	10	88^o	2^o
125 km	$NO^+, 0_2^+$	1	1	10^3	50^o	11^o
130 km	$NO^+, 0_2^+$	1	1	10^3	39^o	11^o
135 km	$NO^+, 0_2^+$	1	1	10^3	33^o	7^o
150 km	$NO^+, 0_2^+, 0^+$	1	1	10^3	19^o	4^o
180 km	$NO^+, 0_2^+, 0^+$	1	1	10^3	7^o	3^o
200 km	$NO^+, 0^+$	1	1	10^4	1^o	3^o
250 km	0^+	1	1	10^4	0^o	0^o

Figure 3

Phase Angle of the Propagation Constants for the Day Ionosphere Model;

Radial B_o = .4 Gauss; Frequency = 13.5 cps

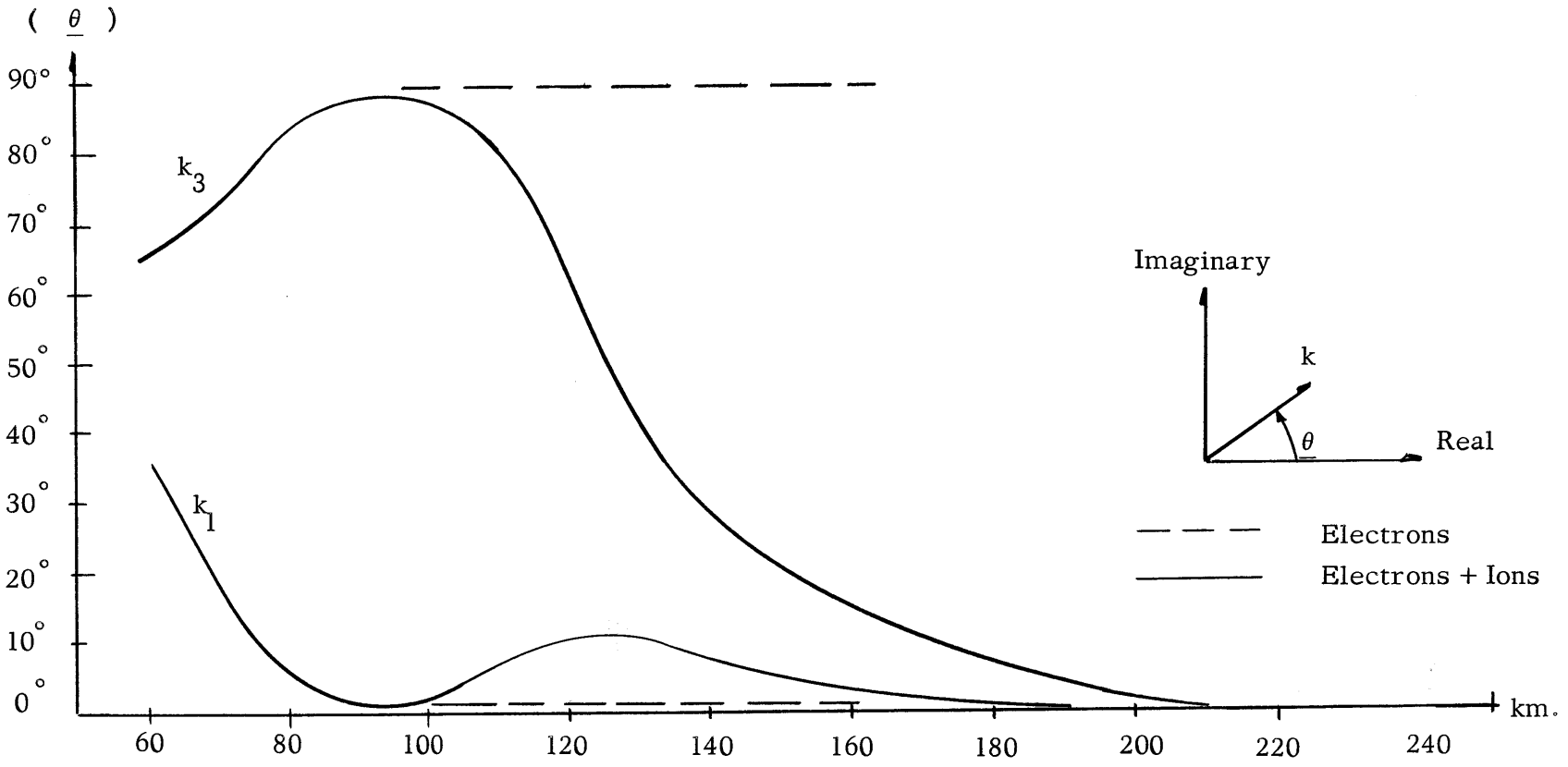

In the 80-100 km region $\sigma_\perp$ is becoming more dependent on the positive ion density and less on that of electrons. Although this is true, computation shows that σ_x dominates the propagation vector, being an order of magnitude greater than $\sigma_\perp$ at 100 km. The third column gives the magnitude of $\sigma_x/\sigma_\perp$ taking into account electrons and an equal number of positive ions. Since the ions as yet have little influence on σ_x, propagation is still very similar to a model in which ion density was neglected.

In the 100-150 km range the NO^+ and O_2^+ ions are of equal importance, judging from the rocket measurements. However, since they both have the same charge and nearly equivalent mass, the conductivity assuming all the ions are NO^+ is not in serious error. Now the affect of the ions on σ_x is equal to that of electrons, while ions completely overpower electrons in $\sigma_\perp$. The phase of k_3 is falling from 90^o towards 0^o, while that of k_1 rises above 0^o to a maximum of about 11^o, then decreases.

By the time an altitude of 250 km is reached O^+ is the significant ion and the phase of both k_1 and k_3 approaches 0^o, though the two k's maintain different magnitudes.

Figure 3 shows the phase changes in the two modes of propagation as a function of height. Only above 100 km do the ions effect a deviation from a purely electron populated profile. Since k enters the wave solutions as exp [ikr], a 90^o phase angle of k_1 or k_3 represents pure attenuation, while 0^o has no attenuation. In the absence of a magnetic field both k_1 and k_3 would merge to one k at 45^o for all altitudes.

k_3 passes through a region of substantial damping from 100-200 km, so it is likely that this wave will be completely attenuated by 200 km. It is possible that energy in the k_1 wave will reach 200 km. If such is the case, then it will propagate much higher because the phase of k_1 approaches 0^o at 250 km.

The computations in Table I were carried out for a B field of .4 gauss. As the field decreases, the conductivity approaches σ_{11}.

In the region below 100 km $\nu_e \sim 15\ \nu_i$ and $m_i \nu_i \gg m_e \nu_e$. An ion density of 50 times the electron density would be necessary to make a 1% change in σ_{11} for the isotropic case.

On the basis of the conclusions outlined in this section, the day model will ignore the presence of ions below 70 km, and above this altitude it will take the positive ion density equal to that of electrons.

4.4 Ions in the Night Ionosphere

In the night ionosphere during quiet solar periods the Lyman alpha zone of electrons does not extend below 85 km [Moler, 1960; Bourdeau, 1962]. The night flux of cosmic rays, however, does produce electron densities of $10/cm^3$ at 80 km, decreasing to near zero at 60 km. The large differences in electron density between the day and night ionosphere in this zone are due to the attachment of cosmic ray produced electrons to O_2 molecules at night and subsequent photodetachment during the day. Therefore the ion density in this region greatly exceeds that of electrons, possibly to the extent that it will result in a substantial conductivity. To examine this possibility we consider the data presented in Figure 5 of Moler [1960] and Figure 2 of Nicolet and Aikin [1960].

At 60 km Moler shows that virtually all the electrons present during the day attach at night. If n^+ (number density of positive ions) remains at its day value given by Nicolet and Aikin, then at night we should have $n^+ = n^- \cong 10^3/cm^3$ (n^- is the density of negative ions). If the ions present are O_2^+, N_2^+ and O_2^-, and taking ν_{in} as $2\ 10^6\ sec^{-1}$, then $\sigma_\perp \cong 1/2\ 10^{-9}$. $(ohm\text{-}meters)^{-1}$. This is equivalent in conductivity to an electron density of $1/cm^3$ at this height and is small enough to be neglected.

At 70 km the night electron density is still less than $10/cm^3$ and again nearly all the day electrons attach at night. Taking $n^- = n^+ \cong 10^3$ and $\nu_i = 5 \cdot 10^5\ sec^{-1}$, then $\sigma_\perp \cong 2 \cdot 10^{-9}$. This ion density is equivalent to an electron density of only $1.5/cm^3$ and is again small enough to be neglected in the conductivity.

These estimates of $\sigma_\perp$ due to the ions should represent an upper limit since it was assumed there was no decrease in n^+ from the day value, and that all the electrons present during the day attach to form negative ions at night. The ion contribution to σ_x is even less important than for $\sigma_\perp$ since the cross-currents due to ions of opposite sign tend to cancel.

At 80 km Moler shows the cosmic ray-produced night electron density at mid-latitudes reaching $10/cm^3$. In the absence of ions this is the altitude at which the model profile would begin. Moler also shows that only about 15% of the electrons present during the day remain at night. Therefore $n^-/n_e \sim 5$ and $(n^- + n^+)/n_e \sim 11$. This will make a 20% change in $\sigma_\perp$ computed just for electrons and no change in σ_x. Since at this altitude $\sigma_x \sim 10\ \sigma_\perp$, the ions can only make a 2% change in k^2.

Therefore ions need only be considered above 85 km where the electron density becomes significant. The nighttime composition of ions [Bourdeau, 1962] is very similar to that during the day.

The above estimates are valid for the entire range of geomagnetic field strength. Below 80 km $\nu_i \gg \omega, \Omega_4$; so $\sigma_\perp \sim \sigma_{11} \gg \sigma_x$ (for ions) even when the B field is .4 Gauss.

4.5 The Transition to Alfven Waves

The low frequencies characteristic of the cavity modes are close to the transition region between electromagnetic and hydromagnetic propagation. The Appleton expression for the index of refraction extended to include positive ions and the Maxwell equations sufficiently describe the waves below 250 km where the cavity problem will be terminated. All the model results for the spherical problem will be for longitudinal propagation where $k^2 = \frac{\omega^2}{v^2} = k_\perp^2 \pm ik_x^2$. At 300 km $\nu_i \cong .2 \text{ sec}^{-1}$, $\nu_e \cong 700 \text{ sec}^{-1}$. For B = .4 Gauss, $\Omega_H \cong 240$ rad/sec and $\omega_H \cong 7 \times 10^6$ rad/sec. For frequencies a decade lower than the lowest cavity frequency $\Omega_H \gg \nu_i, \omega$ and $\omega_H \gg \nu_e, \omega$. Therefore, when $N_e = N^+ (0^+ \text{ ions})$

$$\sigma_x \cong Ne^2 \left[-\frac{1}{m_e \omega_H} + \frac{1}{m_i \Omega_H (1 - \omega^2/\Omega_H^2)} \right]$$

$$= \frac{Ne^2}{m_i} \frac{\omega^2}{\Omega_H^3}, \quad \text{since } m_e \omega_H = m_i \Omega_H \qquad 4.5.1$$

$$\sigma_\perp \cong \frac{Ne^2}{m_i} \frac{(\nu_i - i\omega)}{\Omega_H^2} \qquad 4.5.2$$

Now as the altitude increases, $\omega \gg \nu_i$, so

$$\sigma_x \rightarrow \frac{Ne^2}{m_i} \frac{\omega}{\Omega_H^2} \left(\frac{\omega}{\Omega_H}\right) \qquad 4.5.3$$

$$\sigma_\perp \rightarrow \frac{Ne^2}{m_i} \frac{\omega}{\Omega_H^2} (-i) \qquad 4.5.4$$

Since $\Omega_H \gg \omega$, $\sigma_\perp \gg \sigma_x$ and

$$k^2 \cong k_\perp^2 = i\mu\omega\sigma_\perp = \frac{\mu\omega^2 N m_i}{B^2} = \frac{\omega^2}{v^2} \qquad 4.5.5$$

or, $$v^2 = \frac{B^2}{\mu N m_i}$$

which is the velocity obtained from Alfven's formula using only the density of charged matter.

4.6 The Conductivity Resonance

The expressions for $\sigma_\perp$ and σ_x are clearly frequency dependent, and at high altitudes (200 km and above) they exhibit a resonant phenomenon which could have profound affects on the wave propagation. This resonance is due entirely to the ionic term in the conductivity at 200 km and above, where $\Omega_H^2 \gg \nu_i^2$,

$$\sigma_x = \underbrace{-\frac{Ne}{B}}_{\text{(electrons)}} + \frac{Ne}{B} \times \frac{1}{\underbrace{1 - \frac{\omega^2}{\Omega_H^2}}_{\text{(ions)}} - \frac{2i\omega\nu_i}{\Omega_H^2}} \qquad 4.6.1$$

$$= \left[\sigma_x\right]_{el} \cdot \left[1 - \frac{1}{1 - \frac{\omega^2}{\Omega_H^2} - \frac{2i\omega\nu_i}{\Omega_H^2}}\right] \qquad 4.6.2$$

where $\left[\sigma_x\right]_{el} = \sigma_x$ for electrons only.

Writing $A = \frac{\omega}{\Omega_H}$ and $B = \frac{\nu_i}{\Omega_H}$

the real and imaginary parts of σ_x are

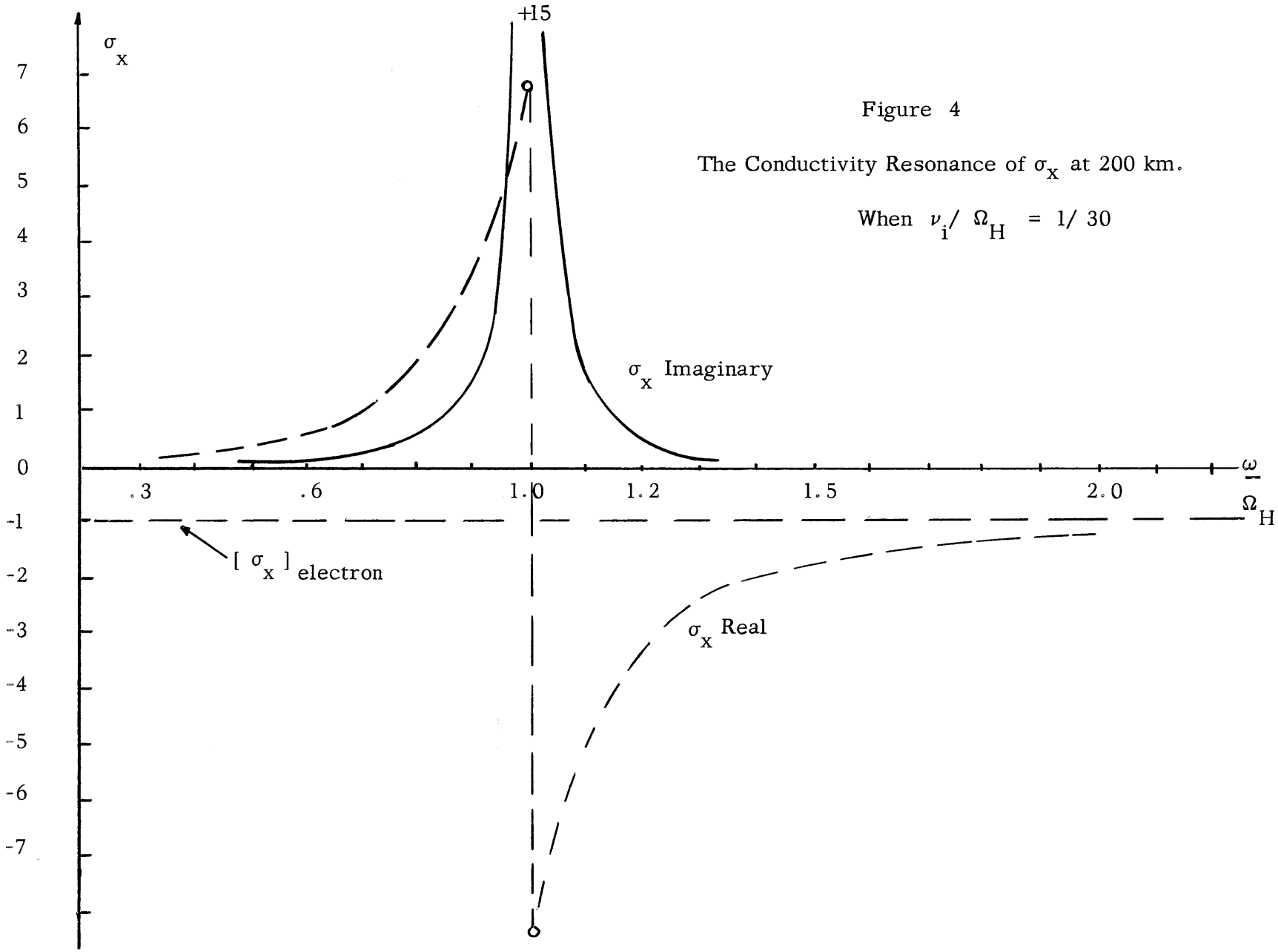

Figure 4

The Conductivity Resonance of σ_x at 200 km.

When $\nu_i / \Omega_H = 1/30$

$$\left[\sigma_x\right]_R = \left[\sigma_x\right]_{el.} \left[1 - \frac{1 - A^2}{(1 - A^2)^2 + 4A^2B^2}\right] \qquad 4.6.3$$

$$\left[\sigma_x\right]_I = \left[\sigma_x\right]_{el.} \left[\frac{-2AB}{(1 - A^2)^2 + 4A^2B^2}\right] \qquad 4.6.4$$

$\left[\sigma_x\right]_R$ has peaks when $A^2 = 1 \pm 2B$, or when $\omega^2 = \Omega_H^2 \pm 2\nu_i \Omega_H$.

$\left[\sigma_x\right]_I$ peaks at $A = 1$, or $\omega = \Omega_H$.

Figure 4 is a plot of the real and imaginary parts of σ_x for the slightly damped case of $\Omega_H = 30\ \nu_i$, which is roughly the case at 200 km. When B = .4 Gauss, $\Omega_H \cong 240$ rad/sec which, at 38 cps, is above the anticipated fourth mode frequency of 26.5 cps. Decreasing the B field, however, lowers the resonant frequency Ω_H right into the range of the first four cavity modes. The vertical scale in Figure 4 is normalized to $\left[\sigma_x\right]_{el.} = -1$. At higher altitudes where $\nu_i \to 0$, $\left[\sigma_x\right]_I \to 0$ and $\left[\sigma_x\right]_R \to$ infinity at $\omega = \Omega_H$.

Since $\sigma_\perp$ has the same denominator as the ion part of σ_x, it behaves the same way. The question of interest is whether the index of refraction exhibits similar behavior.

For longitudinal propagation

$$k^2 = \mu\omega\,(i\sigma_\perp \mp \sigma_x)$$

$$\text{or } k^2 = i\mu\omega\left[\frac{N_e^2}{m_e}\,\frac{(\nu_e - i\omega) \mp i\omega_H}{(\nu_e - i\omega)^2 + \omega_H^2} + \frac{Ne^2}{m_i}\,\frac{(\nu_i - i\omega) + i\Omega_H}{(\nu_i - i\omega)^2 + \Omega_H^2}\right]$$

$$k_1^2 \text{ (top sign)} = i\mu\omega\left[\frac{N_e^2}{m_e}\,(\nu_e - i\omega + i\omega)^{-1} + \frac{N_e^2}{m_i}\,(\nu_i - i\omega - i\Omega_H)^{-1}\right]$$

$$k_3^2 \text{ (bottom sign)} = i\mu\omega\left[\frac{N_e^2}{m_e}\,(\nu_e - i\omega - i\omega_H)^{-1} + \frac{N_e^2}{m_i}\,(\nu_i - i\omega + i\Omega_H)^{-1}\right]$$

where Ω_H is a positive number. There is no resonance to the electron conductivity since $\omega_H \gg \omega$. Also, since Ω_H is positive, there is no resonance to k_1. There is, however, for k_3 when $\omega \cong \Omega_H$ for small ν_i. Reference to Figure 3 will show that k_3 is the wave which is more heavily damped in the 100-200 km zone.

Numerical results show that this zone is only on the order of several skin depths deep at 14 cps in the night ionosphere with radial $B_0 = .4$ Gauss. This means that an appreciable portion of low frequency cavity energy in the k_3 wave can reach this altitude. The problem of the k_3 wave encountering a conductivity resonance is avoided, however, as is apparent from skin depth results in Chapter 5. For a B field of .4 Gauss the highest mode frequencies discussed are below the ion gyrofrequency by about 10 cps. Decreasing the magnitude of the B field lowers the gyrofrequency, but it also decreases the skin depth for the k_3 wave. By the time Ω_H is comparable to ω, the wave energy is either damped out or reflected before it can reach an altitude where ν_i is small enough to allow a conductivity resonance.

There is enough damping and reflection below 200 km in the day model so that cavity waves will not penetrate into the region of possible conductivity resonance, even for the case of a radial B field of .4 Gauss.

CHAPTER V

NUMERICAL RESULTS AND CONCLUSIONS FOR N-LAYER MODELS

This chapter presents the machine computation results for several cavity models which will illustrate both qualitatively and quantitatively the affect of the geomagnetic field on the resonant mode properties and also on the nature of the propagation of the cavity waves. Models range in complexity from several layers in the cylindrical cavity to 50 or 60 layers in the spherical cavity for the night ionosphere where the anisotropic conductivity allows propagation to altitudes of over 200 km.

5.1 The Cylindrical Model

Since this model will be used primarily to predict general results of the cavity modes rather than the more specific results left to the spherical problem, several simplifications are allowed in defining the conductivity profile. The ionosphere above 100 km will be treated as one layer of constant properties. Certainly this does not fit the real case, but it will not alter any of the conclusions to be drawn here. Figure 5 illustrates how the model electron density profile fits the data of Moler [1960] (dotted curve). Only electrons are considered in this case; therefore, this description is limited to the real cavity properties below 100 km where ions are unimportant. The conductivity computations at the bottom of Figure 5 were made using a collision frequency appropriate to the middle of each layer, and $B_0 = .44$ Gauss. In Zone III $\nu_e = 2 \cdot 10^4$ sec^{-1}. which is appropriate at about 115 km.

Table II summarizes the numerical results of the cylindrical cavity. Cases a and b are done for a radial B field of .44 Gauss, cases c and d for the isotropic problem, and case e for an axial B field. Case e is seen to be equivalent to propagation around the equator, since the propagation direction both in the air and in the ionosphere is always perpendicular to the geomagnetic field. Cases b and e use the same conductivity profile; the wave solutions are different due to a different magnetic field direction.

The following observations are made of Table II results. Identical results for cases c and d indicate that the wave energy in the isotropic case never reaches as high

Figure 5

Three Layer Model Fit to the Noon Ion Density
of Moler (1960)
The Cylindrical Cavity Resonance Problem

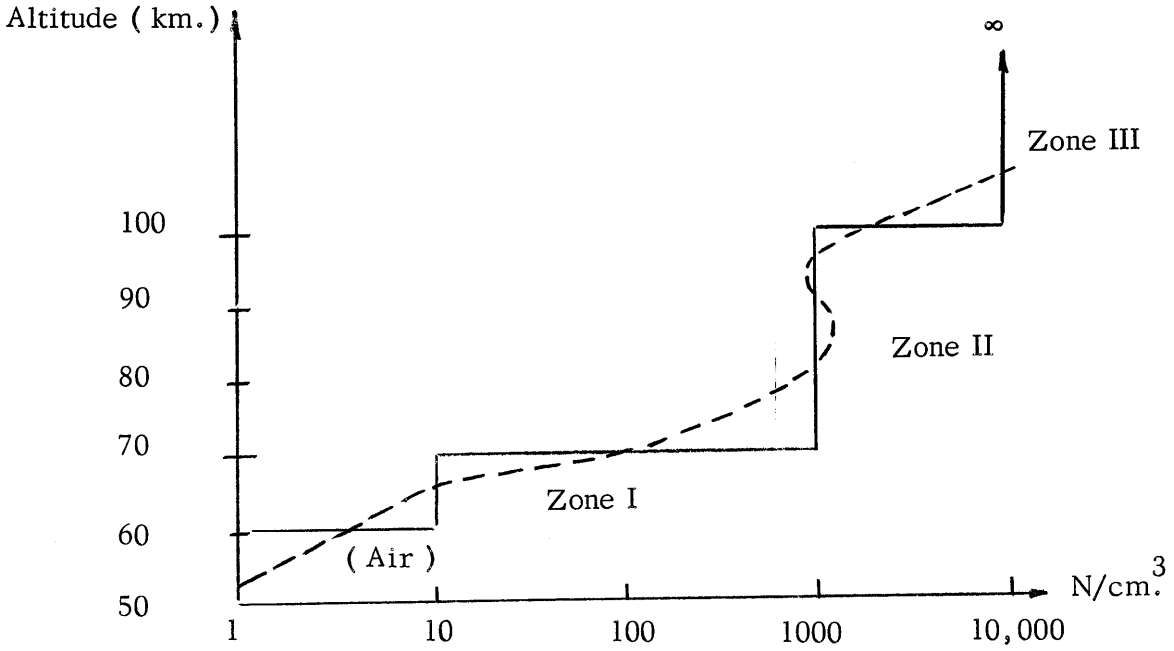

Zone I	Zone II	Zone III
$\sigma_{\perp} = 1.8 \times 10^{-8}$	$\sigma_{\perp} = 1.7 \times 10^{-7}$	$\sigma_{\perp} = 1.0 \times 10^{-6}$
$\sigma_{x} = 1.4 \times 10^{-8}$	$\sigma_{x} = 7.0 \times 10^{-6}$	$\sigma_{x} = 7.0 \times 10^{-5}$
$\sigma_{11} = 2.9 \times 10^{-8}$	$\sigma_{11} = 2.9 \times 10^{-4}$	$\sigma_{11} = 4.9 \times 10^{-3}$

Conductivities are determined using the collision frequency appropriate to the altitude at the middle of each zone.

TABLE II

Model Results for 3-Layer Cylindrical Problem

Mode Order	n = 1 f_o, Q	n = 2 f_o, Q	n = 3 f_o, Q	n = 4 f_o, Q
a. $B_0 = B_r$ = .44 Gauss Perfect Reflector at 100 km	5.8, 40	11.5, >100	17.1, >100	22.5, >100
b. $B_0 = B_r$ = .44 Gauss Zone III of Finite Conductivity	5.6, 8	11.3, 9	17.1, 9	22.8, 8
c. $B_0 = 0$ Perfect Reflector at 100 km	6.65, 15	13.4, 19	20.2, 22	27.1, 24
d. $B_0 = 0$ Zone III of Finite Conductivity	6.65, 15	13.4, 19	20.2, 22	27.1, 24
e. $B_0 = B_z$ = .44 Gauss Zone III of Finite Conductivity	6.1, 14	12.5, 16	18.8, 17	25.3, 19

as 100 km, since changing Zone III from a finite conducting layer to a perfect reflector at 100 km has no affect on the cavity response.

When a radial B field of .44 Gauss is introduced, several important changes occur. The cavity losses which had been dissipative in the isotropic case are now due primarily to energy leaking out of the cavity. The Q's in case a are higher than in case c because less energy is dissipated below 100 km, and none of it can escape the cavity due to the perfect reflector at the top. Case b has lower Q's than either case a or c because the energy is now propagating in non-dissipative modes which leak out of the cavity with less reflection at each layer boundary than in the isotropic case.

The presence of the geomagnetic field has also caused a general lowering of the resonant frequencies by about n cycles for the n^{th} mode, as can be observed by comparing cases b and c. Only slight frequency differences occur between cases a and b; it is mainly the difference in the Q's in these two problems which gives a measure of the importance of considering the ionosphere above 100 km in the anisotropic problem. Comparison of cases b and e gives a measure of the effect of changing the geomagnetic field from radial to axial. The resonant frequencies in the axial case have increased by roughly $\frac{n}{2}$ cycles for the n^{th} mode over the radial field case, and the Q's have approximately doubled. Clearly the axial field results are closer to the isotropic case than the radial field results. Indeed, it was pointed out in Chapter IV that when only electrons contribute to the conductivity, $k_p = k_{11}$ (where $k_p^2 = k_\perp^2 + k_x^4/k_\perp^2$). The wave solutions for cases d and e remain different, but both problems support only a TE mode with a propagation constant equal to k_{11}. Analytical results indicate that for a single infinite layer ionosphere cases d and e should give identical results for just electrons.

A simple extrapolation in the case b of a radial field can be made to translate frequencies of the cylindrical cavity to a spherical one by multiplying by the factor $\sqrt{n(n+1)}/n^2$. If this is done the first four cavity frequencies of case b become 7.9, 13.8, 19.7, and 25.6 cps, respectively. These are at least comparable to the measured peaks of Balser and Wagner [1960].

The fact that energy dissipation is higher in the isotropic media than the anisotropic one can be explained as follows. Writing $J_i = \sigma_{ij} E_j$ and using the σ_{ij} given by Equation (1.3.10) for a radial B field,

$$\text{(a)}\ J_r = \sigma_{11} E_r$$

$$\text{(b)}\ J_\theta = \sigma_\perp E_\theta + \sigma_x E_z \qquad 5.1.1$$

$$\text{(c)}\ J_z = -\sigma_x E_\theta + \sigma_\perp E_z$$

Reference to Equations (C.2.4) in Appendix II indicates that $E_\theta = \mp i E_z$ 5.1.2

Applying (5.1.2) to (5.1.1),

$$J_\theta = E_\theta (\sigma_\perp \pm i\sigma_x)$$

$$J_z = E_z (\sigma_\perp \pm i\sigma_x) \qquad 5.1.3$$

The dissipation losses of a medium are given by

$$P = \iiint_\tau J \cdot E \, d\tau \qquad \text{where } \tau = \text{volume}$$

Now J and E are both complex vector functions of position and time. If we average the losses over time, then

$$J \cdot E = \frac{1}{2} [E_R \cdot J_R + E_I \cdot J_I] \qquad 5.1.4$$

where R and I denote the real and imaginary parts of the vectors E and J. If we define $\bar{E}$ as the complex conjugate of E, then

$$J \cdot E = \frac{1}{2} R_e \, J \cdot \bar{E} \qquad 5.1.5$$

Substituting expressions (5.1.1-a) and (5.1.3) into (5.1.5),

$$J \cdot E = \frac{1}{2} R_e \left[\sigma_{11} |E_r|^2 + (\sigma_\perp \pm i\sigma_x) (|E_\theta|^2 + |E_z|^2) \right] \qquad 5.1.6$$

where $E_r \bar{E}_r = |E_r|^2$, etc.

In the isotropic case where only the TE mode is excited

$$J \cdot E = \frac{1}{2} R_e \left[\sigma_{11} \left(|E_r|^2 + |E_\theta|^2 \right) \right] \qquad 5.1.7$$

As an example to compare (5.1.6) and (5.1.7) we shall evaluate $J \cdot E$ at 100 km in the two cases. The collision frequency at this altitude is still high enough so that the conductivity terms are real. Therefore (5.1.6) becomes

$$J \cdot E = \frac{1}{2} \sigma_\perp \left(|E_\theta|^2 + |E_z|^2 \right) + \frac{1}{2} \sigma_{11} |E_r|^2 \qquad 5.1.8$$

where E_θ and E_z are the same order of magnitude.

At 100 km for a B field of .4 Gauss $\sigma_\perp \sim 10^{-8}$, $\sigma_x \sim 10^{-6}$ and $\sigma_{11} \sim 10^{-4}$. Although E_r is a factor of (kr) smaller than E_θ or E_z, σ_{11} is large enough compared with $\sigma_\perp$ to make the longitudinal and transverse losses of (5.1.8) the same order of magnitude.

In the isotropic case $E_r \ll E_\theta$, so

$$J \cdot E = \frac{1}{2} \sigma_{11} |E_\theta|^2 \qquad 5.1.9$$

Since $\sigma_{11} \gg \sigma_\perp$ (the factors of $|E_\theta|^2$) the losses are much greater for the isotropic case. This applies to both anisotropic modes.

Figures 6 and 7 show a sample plot of the frequency structure of the modes for the axial magnetic field case. The program prints out the magnitude of one of the field components (tangential H) measured at the earth's surface as a function of frequency for each value of mode number n. The problem treats each mode as if it were the only one excited; therefore there is no reason why the plots for n = 1 and n = 2, say, should have the same amplitude at 9 cps. The power overlap of adjacent modes is sufficiently small to make only a negligible change in the peak frequency and Q of any particular mode. The delta function source in the model puts an equal amount of energy into each mode.

Figure 6

Amplitude Spectrum for the Cylindrical Model; Axial B_o = .44 Gauss

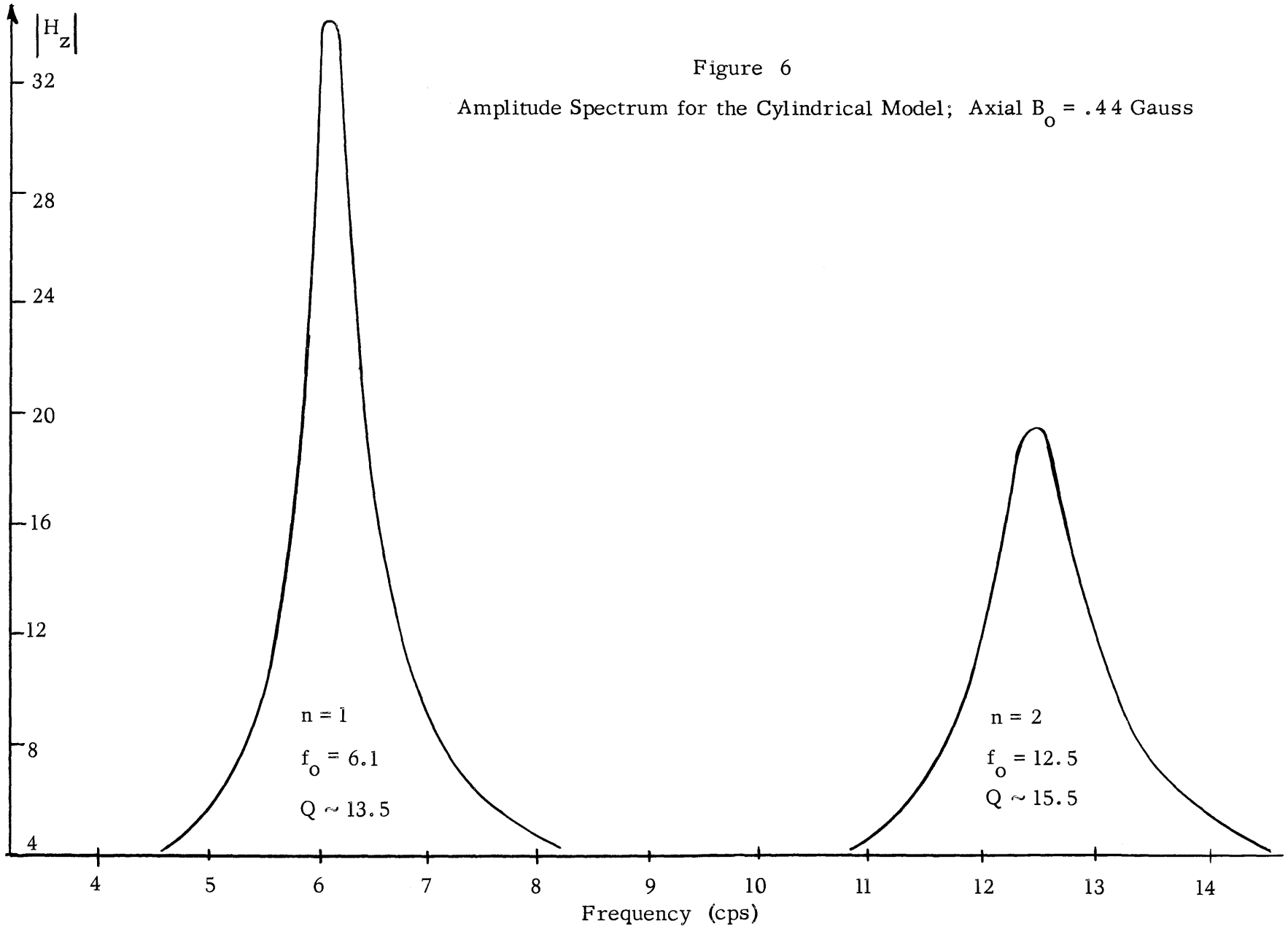

Figure 7

Amplitude Spectrum for the Cylindrical Model; Axial B_o = .44 Gauss

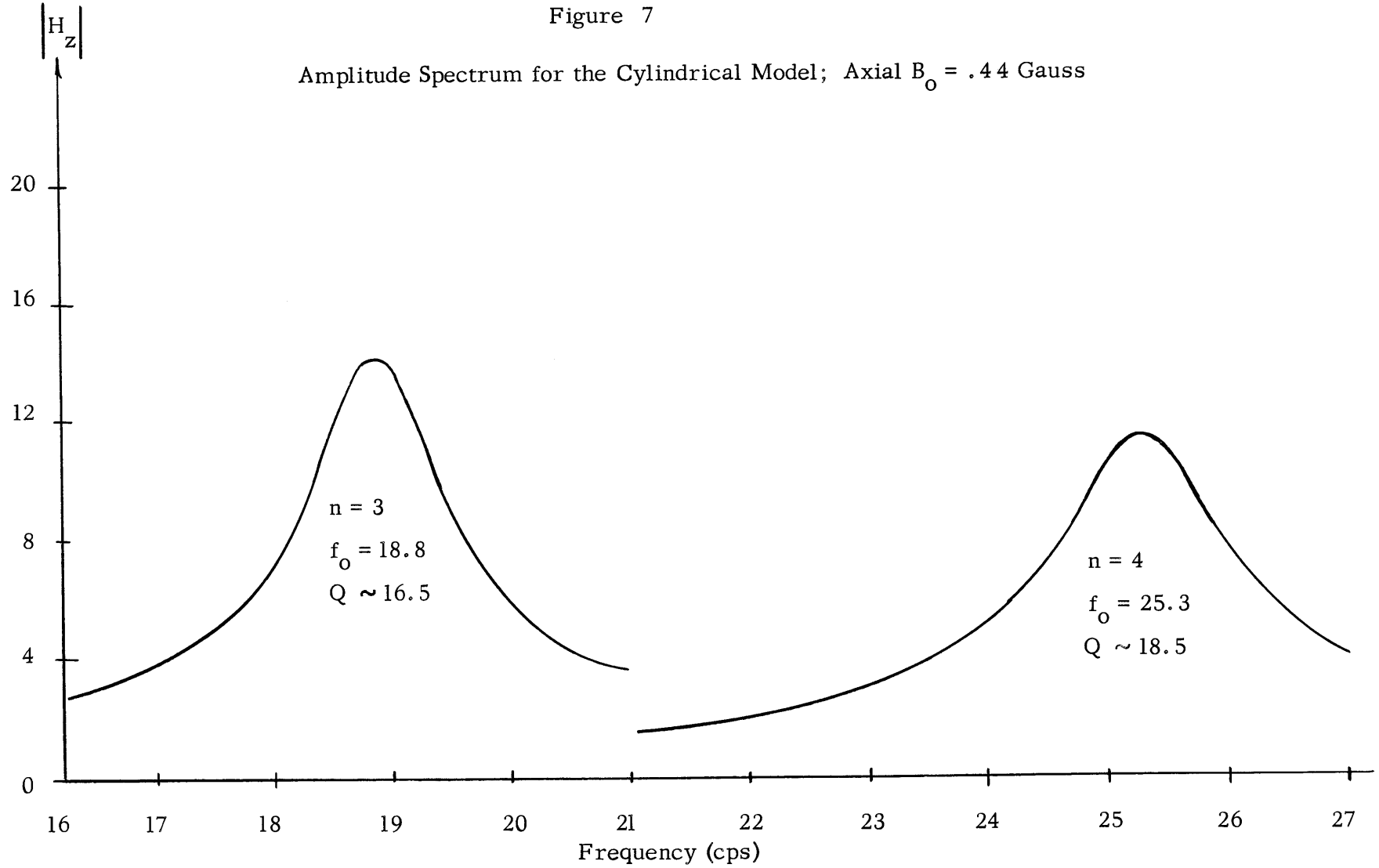

5.2 The Spherical Model

As was pointed out earlier, solutions for the cavity modes of this model are limited to the case of longitudinal propagation. This fits the real ionosphere only in the vicinity of the magnetic poles, where the field is indeed radial. Furthermore, since the model properties only change from one spherical shell to the next, being constant within each shell, only radial conductivity differences are included. An estimate of the average mode properties of the real cavity will be made by considering the extreme cases of completely day or night ionospheres separately. The affect on the results due to the fact that propagation is partially transverse throughout the real cavity will be estimated by extrapolating from the general results of the cylindrical problem.

The conductivity profile was fitted in step fashion to the real data as was done in the cylindrical case, but now with a much closer approximation. It was found that as long as the layer thickness was kept less than one-tenth the shortest wavelength used in each layer, a closer approach to the continuous case by using much thinner layers only changed the amplitude of the response by a few per cent at resonance, and made no change away from the peak. A summary of the data to which the models were fitted will be presented at the end of this chapter.

Analysis of Tables III and IV

Tables III and IV present a summary of the data for a typical noon and night ionosphere under quiet solar conditions. Results are presented for three different strengths of magnetic field: B = .4 Gauss to correspond to polar conditions; B = 10^{-4} Gauss to correspond to isotropic conditions; and B = .2 Gauss to show that there is something of a smooth transition between the two former.

The general increase in peak frequency with decreasing B field, both in the day and night models, is the same trend as was observed in the cylindrical problem. Notice that the magnitude of this change is much more dramatic in the night problem than the day.

The peak frequency of the night model is always higher than the equivalent day case. This can also be observed in the isotropic model of Galejs [1962].

TABLE III

PEAK FREQUENCIES FOR LONGITUDINAL PROPAGATION

		B = .4 Gauss	B = .2 Gauss	B = 10^{-4} Gauss
DAY	n = 1	7.7	7.7	7.9
	n = 2	13.3	13.4	13.8
	n = 3	18.9	19.1	19.6
	n = 4	24.4	24.7	25.4
NIGHT	n = 1	8.5	8.7	9.6
	n = 2	15.0	15.2	16.8
	n = 3	21.5	21.8	23.9
	n = 4	27.8	28.3	30.9

TABLE IV

Q's FOR LONGITUDINAL PROPAGATION

		B = .4 Gauss	B = .2 Gauss	B = 10^{-4} Gauss
DAY	n = 1	14	19	23
	n = 2	19	17	20
	n = 3	20	24	17
	n = 4	17	16	15
NIGHT	n = 1	7	9	17
	n = 2	9	11	18
	n = 3	10	10	19
	n = 4	11	11	23

The day and night results for the case B = .4 Gauss should give the closest fit to the real case when their average is considered. The actual cavity has walls whose surface area is one half day and one half night ionosphere. Therefore the simplest estimate of the average cavity frequencies is to average the day and night peaks, giving 8.1, 14.2, 20.2, and 26.1 cps respectively. These compare favorably with the measured frequencies of 7.8, 14.1, 20.3, and 26.5 cps given by Balser and Wagner [1960].

In a discussion of the Q's presented in Table IV, two points should be considered. First, in the night model, there is a general increase in the Q with decreasing magnetic field, as was the case in the cylindrical problem. In the day model this is only noticeable in the first mode; the Q in higher modes remains roughly the same. Secondly, for the more important case of B = .4 Gauss, the Q is higher for the day model than the night. This is somewhat unexpected since the dissipation losses should be higher for a noon ionosphere due to a higher charge density at any height than at night. The explanation is that the layers in the day ionosphere below 85 km, while they cause some dissipation, also reflect some wave energy back inside the cavity. In a night ionosphere a wave reaches 85 km with no losses, but similarly no reflection. From this height up to 200 km the k_3 wave passes through a region of high enough attenuation both for a day model (see Figure 3) and a night model (see Figure 8) that most of its energy should be dissipated or returned to the cavity. The k_1 wave, however, experiences only minor losses between 100 and 150 km in both models, so there is a chance of this energy leaking out of the cavity and lowering the Q as a result. Model results showed that for a day model cavity energy was confined below 150 km, but for the night model it propagated well above 200 km into the lossless region of real propagation constant. Once energy gets above 200 km, it is lost to the cavity. Therefore the day model has higher dissipation but more energy reflected back into the cavity below 150 km than the night model which was able to save more of its energy from frictional losses only to lose it all in the lossless sink above 200 km.

An explanation of how the height of propagation of cavity energy was determined is in order at this point. All problems were run with both the layer of infinite extent

Figure 8

Phase Angle of the Propagation Constants for the Night Ionosphere Model

Radial B_o = .4 Gauss Frequency = 14 cps

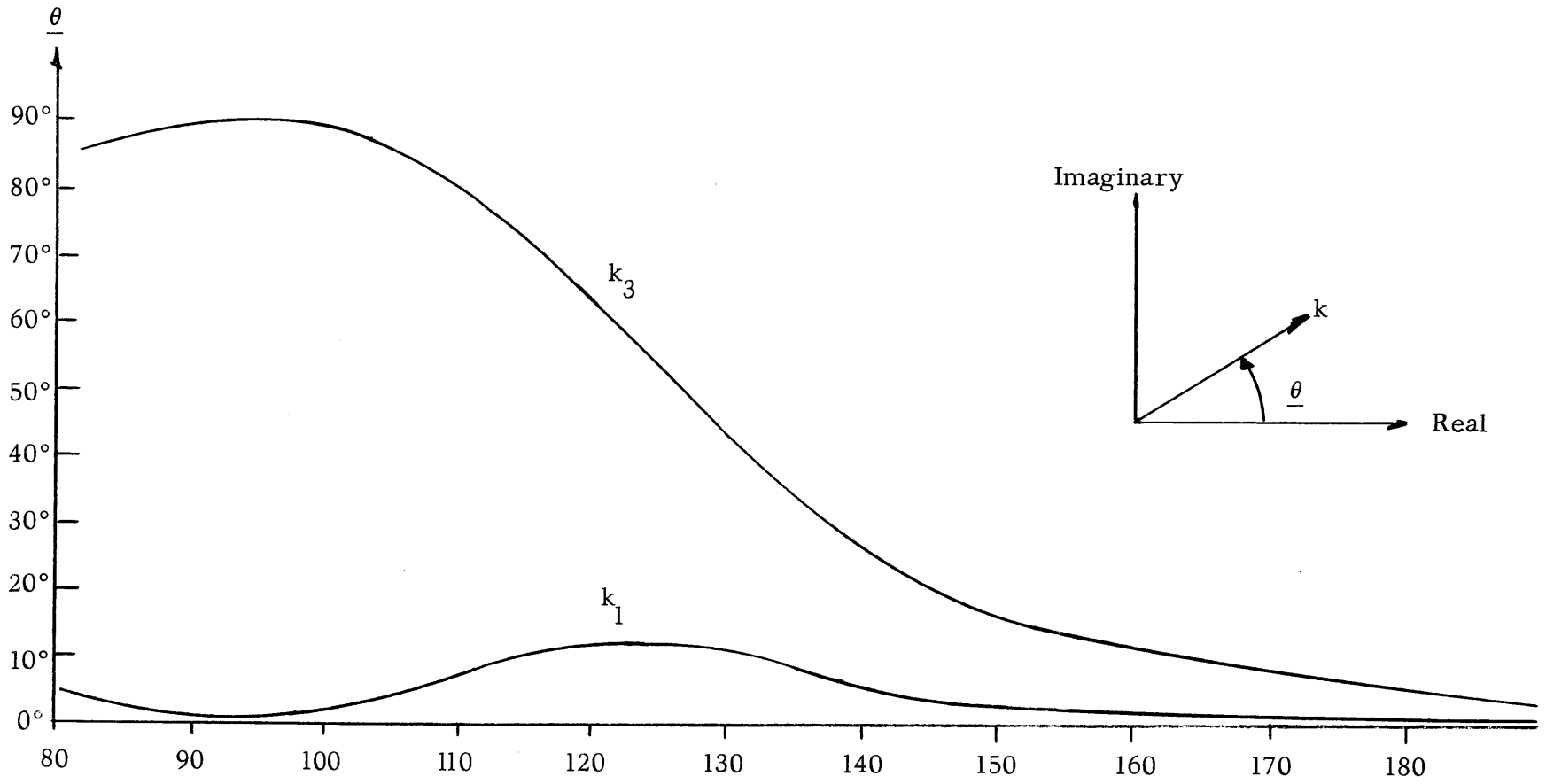

and the perfectly reflecting layer at the top of the model. When the cavity response as determined from the amplitude of H_ϕ agreed to at least two figures in the two cases, it was assumed that an insignificant amount of cavity energy reached that altitude. This figure then is a maximum altitude of penetration. It was 118 km for the night isotropic case, 94 km for the day isotropic case, and 150 km for B = .4 Gauss in the day model. Some argument for these height estimates is presented in the skin depth vs. height graphs of Figures 9, 10, and 11.

Analysis of Figures 9, 10 and 11

Figure 9 shows that in the isotropic problem the skin depth drops to a few kilometers by 90 km in the day and by 110 km at night. Higher frequencies damp out faster as is the case for frequency-independent conductivity. There is only one wave mode present here.

Figure 10 for a day model of .4 Gauss shows the two waves, with k_3 the more heavily damped, as in Figures 3 and 8. Above 100 km the ions play a strong role in determining the propagation constants. The net result is to make both k_1 and k_3 real above an altitude of 250 km. The intermediate region of 100-250 km is one of gradual change towards real propagation constants and longer skin depths. This is really a joint effect due to the presence of the ions and the decreasing ion collision frequency with altitude. The ions make $\sigma_\perp$ comparable in magnitude to σ_x, and the decreasing collision frequency makes $\sigma_\perp$ essentially imaginary above 200 km. At the same time the ion affect is comparable to that of electrons in σ_x, and the decreasing collision frequency makes σ_x real above 200 km. Since $k^2 = \mu\omega(i\sigma_\perp \mp \sigma_x)$, k_1 and k_3 become real and their skin depths correspondingly increase.

Figures 10 and 11 show that for any given height the skin depth for a wave of particular frequency in the day model is shorter than the skin depth for the same wave at night; this is because the charge density is greater during the day.

If the mode energy is not damped out before an altitude of 160 km in the night model, then it is essentially lost to the cavity. The strongest wave at this point would be k_1, and the skin depth at 160 km is several hundred kilometers and still rising. The approximations made in the conductivity derivation are valid up to 400 km in the night

Figure 9

Skin Depth vs. Altitude for a Day and Night Cavity Model

Radial $B_o = 10^{-4}$ Gauss

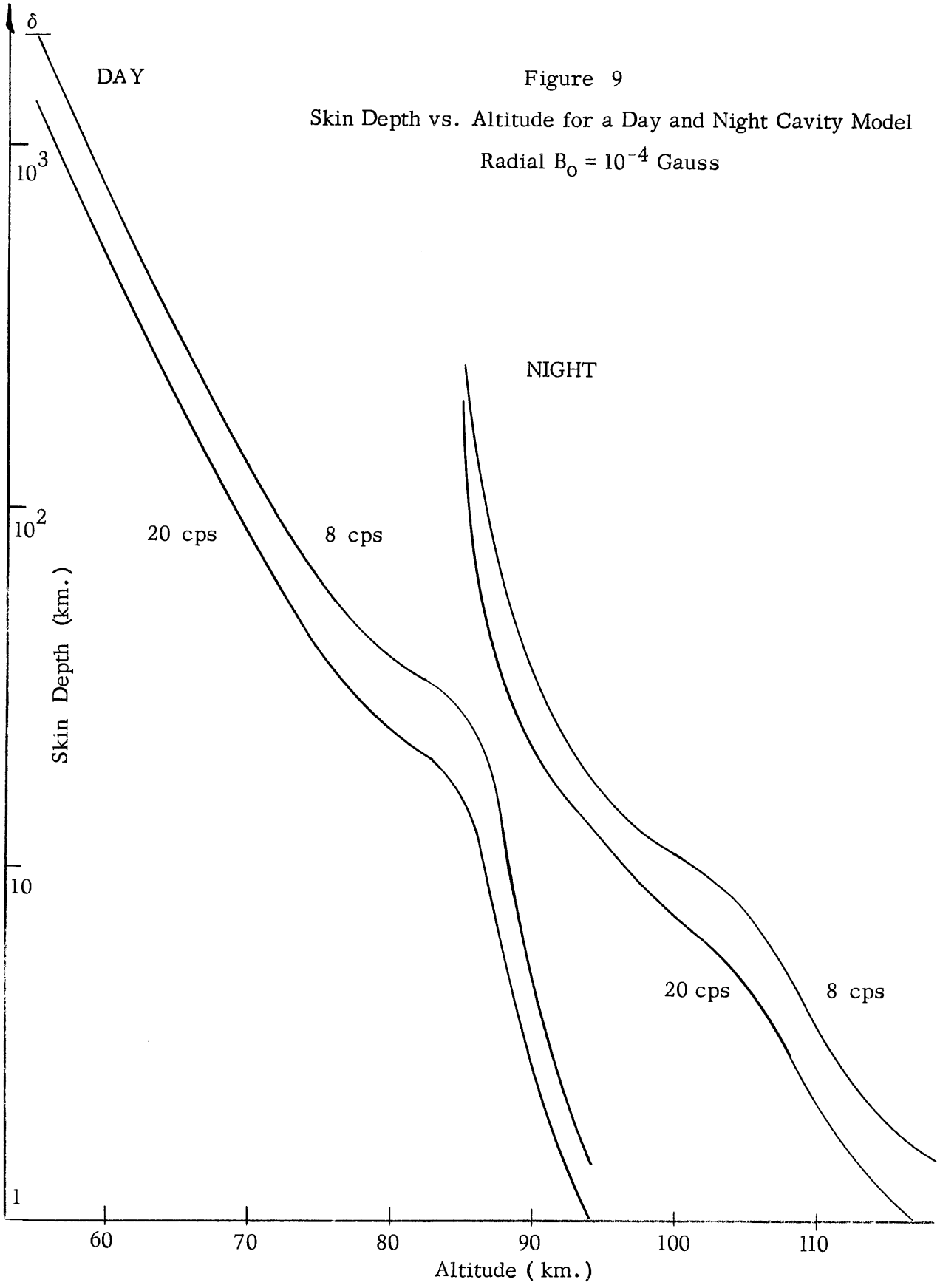

Figure 10

Skin Depth vs. Altitude for the Day Cavity Model

Radial B_o = .4 Gauss

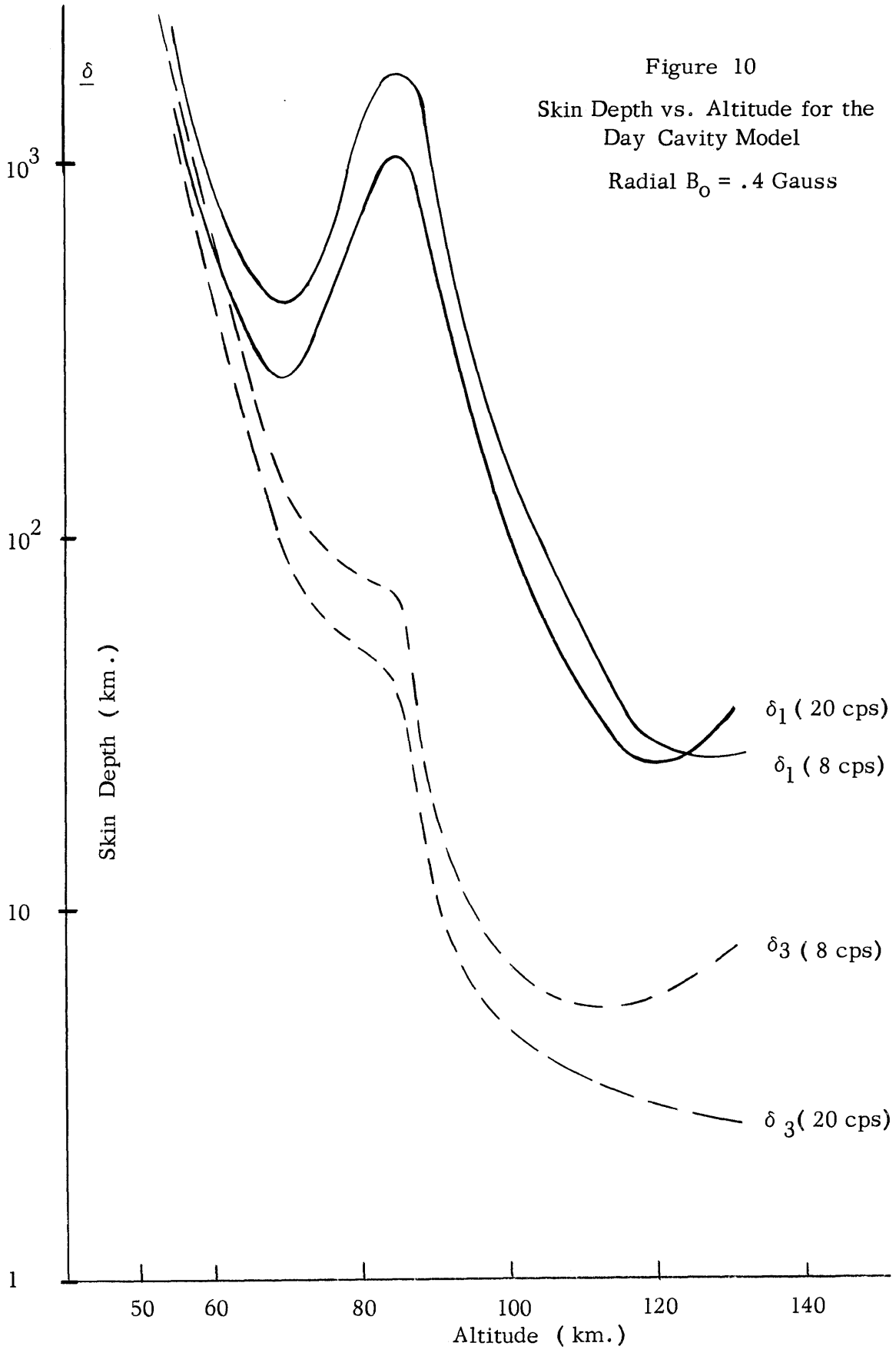

Figure 11

Skin Depth vs. Altitude for the Night Model

Radial B_o = .4 Gauss

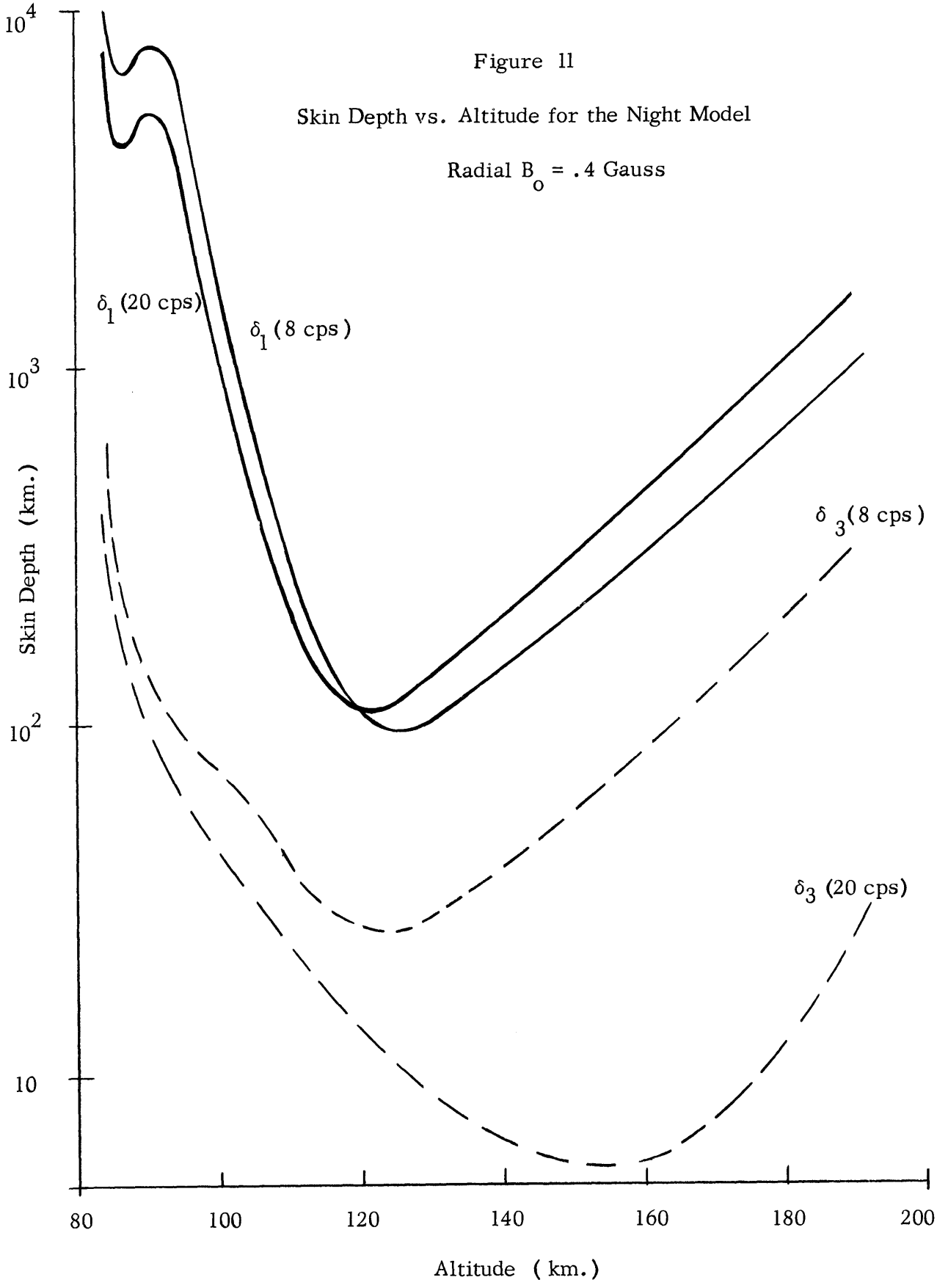

ionosphere. However, extending the model this far is of little value, since the additional lossless region will not help terminate the problem.

Several different terminating layers were used on the night model with B = .4 Gauss. These layers had conductive properties appropriate to various heights between 200 and 300 km and they all produced identical results in the problem.

The δ_1 Cross-over at 120 km

It should be noticed both on Figure 10 and Figure 11 that at about 120 km the skin depth for the 20 cps wave becomes longer than that for the 8 cps wave. This is not due to a conductivity resonance, since only the k_3 wave experiences that. It is, however, due to the frequency dependence of the conductivity. Consider the following table for the night model, B = .4 Gauss.

Altitude	$k_1(8)$	$k_1(20)$	$\theta_1(8)$	$\theta_1(20)$
115 km	$3.33 \cdot 10^{-5}$	$5.12 \cdot 10^{-5}$	10.7^o	8.8^o
124 km	$3.61 \cdot 10^{-5}$	$6.06 \cdot 10^{-5}$	17.4^o	8.1^o

where

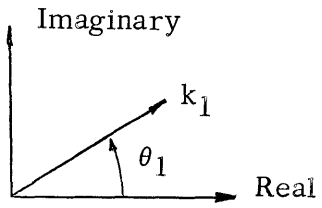

and $k_1(8)$ is the magnitude of k_1 at 8 cps, $\theta_1(8)$ is the phase of k_1 at 8 cps, etc.

Both at 115 km and 124 km the magnitude of k_1 is greater at 20 than at 8 cps. At 115 km k(20) is slightly closer to the real axis than k(8) but its magnitude is still great enough compared with k(8) that $k_I(20) > k_I(8)$; so δ (20) < δ (8). (I indicates imaginary).

At 124 km k(20) is much closer to the real axis than k(8), so even though $k(20) > k(8)$, $k_I(20) < k_I(8)$ and δ (20) > δ (8).

Figure 12

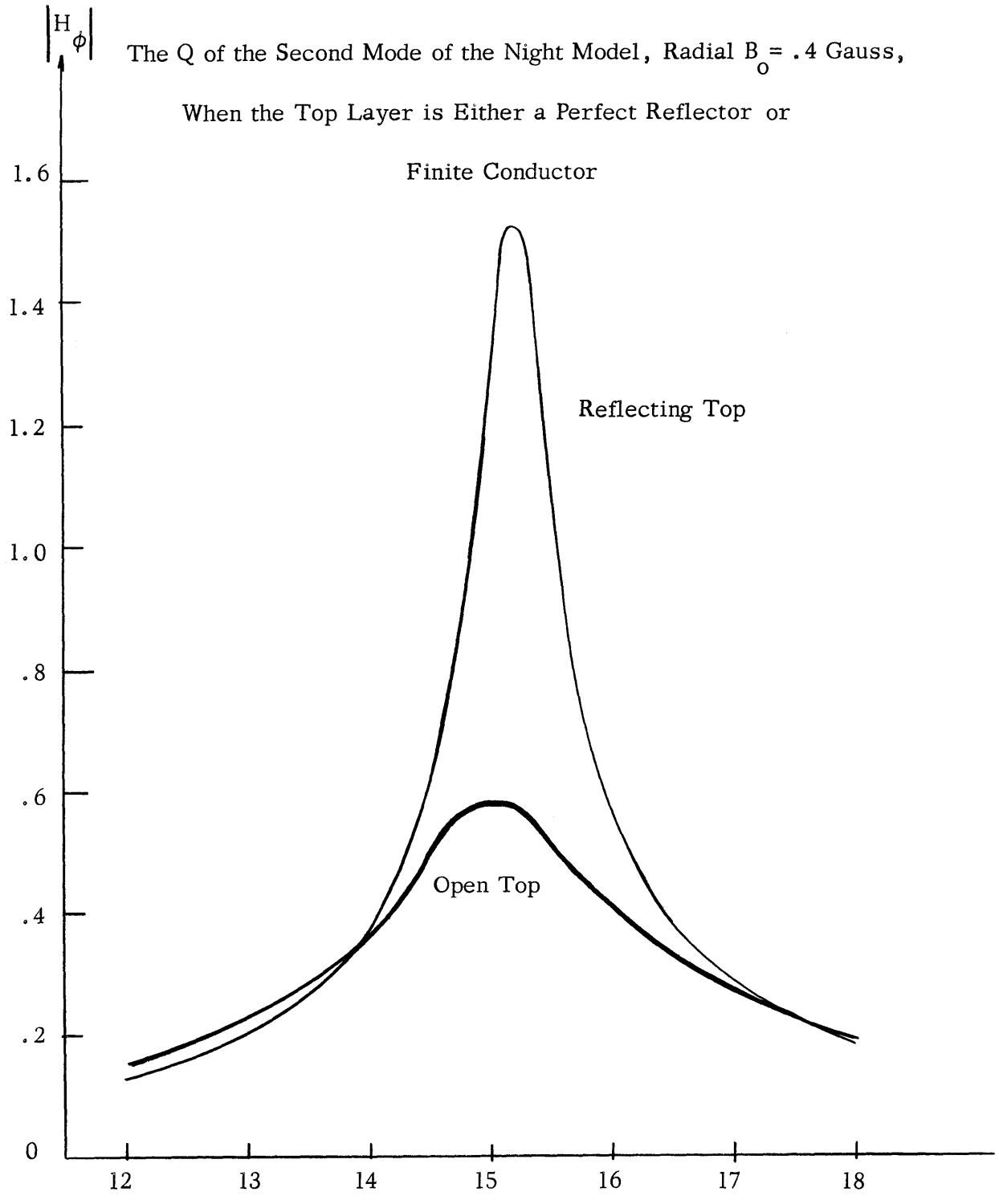
$|H_\phi|$
The Q of the Second Mode of the Night Model, Radial B_o = .4 Gauss,
When the Top Layer is Either a Perfect Reflector or
Finite Conductor
1.6
1.4
1.2
1.0
.8
.6
.4
.2
0
Reflecting Top
Open Top
12
13
14
15
16
17
18
Frequency (cps)

Extent of the Ionosphere which Affects Cavity Waves

It has already been pointed out that the night model with B = .4 Gauss was the one which had so little frictional loss and reflection that a considerable portion of the wave energy leaked out of the cavity. Perhaps one estimate of how much energy is escaping can be obtained by comparing the Q's for models with a reflecting and an open top. This is done for the second mode, as an example, in Figure 12. The Q for the reflecting layer model is about 20, while that for the infinite layer model is about 10. This means that the losses per cycle are twice as great for the open top model, which is more appropriate to the real ionosphere case. In other words, half the losses in the model terminated by an infinite layer are caused by energy leaking out into the lossless medium above 200 km. The reflecting layer was placed at 190 km.

No general statement will be made for all the modes concerning the energy which leaks out of the cavity, since the fourth mode of the reflecting layer problem actually showed a minimum where a peak occurred for the infinite layer solution.

A method to examine more quantitatively the energy distribution in the two waves as a function of height would be to use the results for H_ϕ and H_θ at the earth's surface determined here, and then solve the problem layer by layer for the coefficients of the four waves vs height, the four waves being $\pm k_1$ and $\pm k_3$.

The Affect of Transverse Propagation

The results for the cylindrical problem seem to indicate that the affect of transverse propagation is to shift the peak frequencies toward the isotropic solution, which means a general increase in the values for a model in which propagation is entirely longitudinal. This increase would only improve the fourth mode average results, while raising the frequencies of the first three modes above the experimentally measured average.

General

The mode properties were found by studying the character of H_ϕ, but the same structure is observed in H_θ. H_ϕ was chosen because it is the component excited

Figure 13

The Phase of Tangential $\underline{H}$ Measured at the Earth s Surface for the Second Mode of the Night Model; Radial B_o = .4 Gauss

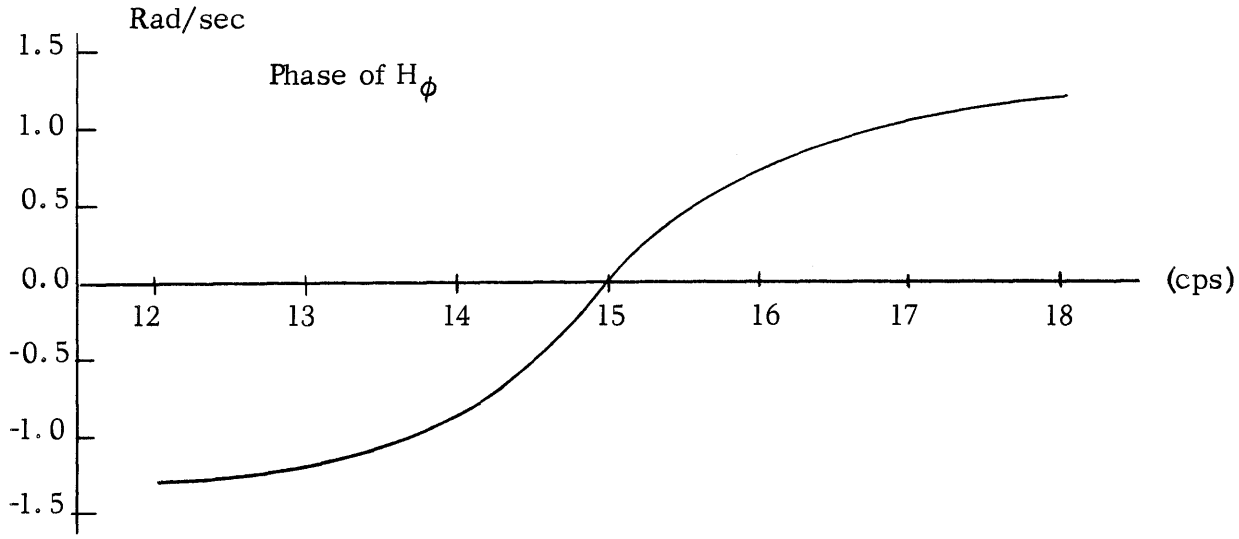

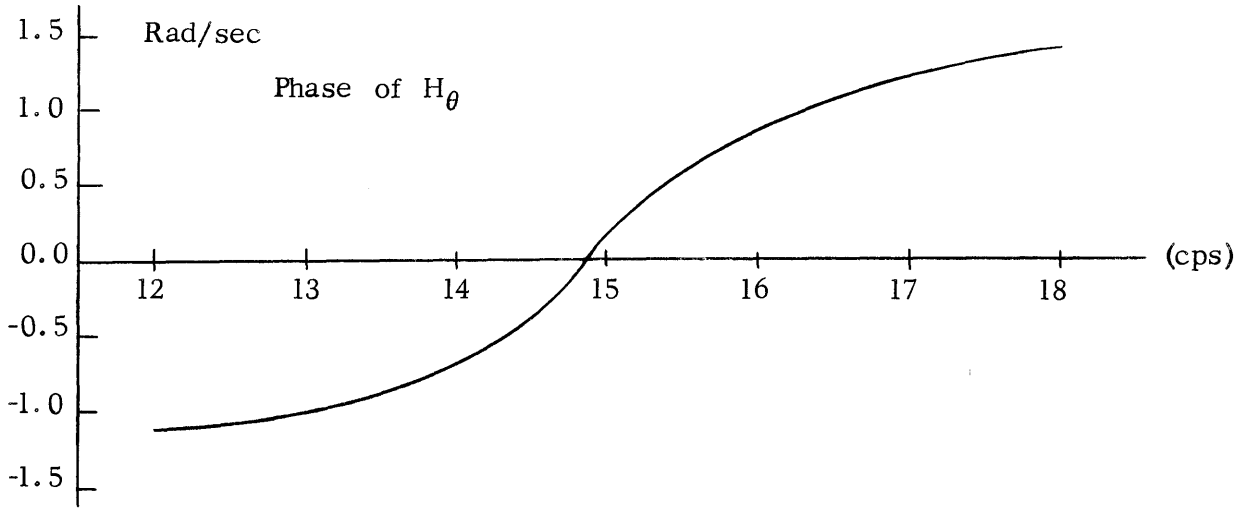

directly by the source and was always an order of magnitude greater than H_θ. The phase of either of these components also indicates the resonant point by where it passes through zero, as indicated in Figure 13. Furthermore, the slope of this curve as it passes through the point of zero phase angle is a qualitative measure of the Q; a greater slope indicates a higher Q, in general.

All observations of mode structure were made on the infinite layer type problem. This model appears closer to the real case than a model with a reflecting top layer.

Figures 14-17 summarize the amplitude spectra for four important models in the spherical case. The data in Tables III and IV comes directly from these figures. Figures 18-21 summarize the data used in the models to determine the conductivity of each layer.

The results of Figures 14-17 express the response of the cavity at a frequency f when the n^{th} mode is excited by a vertical electric dipole of $\exp(-i\,2\pi ft)$ dependence. The computations have assumed a source which was described mathematically as a discontinuity in E_θ of unit magnitude for each frequency and mode. In order to normalize the amplitude spectrum results to the response of a white light source, three factors must be considered.

First, so far as E_θ is concerned, the source is a delta function at $\theta=0$. Spherical harmonic analysis shows that the coefficient for the n^{th} mode of the delta function expansion should be $(2n+1)/2$. Second, examination of the E_θ field indicates that the amplitude of the dipole source term is frequency dependent and is given by $A = I\,ds/4\pi\epsilon_0\omega$, where I and ds are the dipole element current and length, respectively. And third, since the problem treats the modes as independent, the power in the n^{th} mode should be increased by the overlapping power in all the other modes.

The combination of the first two factors leaves the relative peak amplitudes of Figures 14-17 virtually unchanged, since $(2n+1)/f \cong .36$ for n= 1-4. As was mentioned earlier, the overlapping power from adjacent modes makes a negligible change at the mode peaks. The $1/\omega$ factor in A produces a slight shift in peak frequencies towards lower values, but the spectrum Q's are high enough so that this is not more than .1 cps. Raemer [1961] points out that the white light source spectrum should be modified by a factor which decreases exponentially in frequency to fit the power spectrum of the real lightning sources.

Figure 14

Amplitude Spectrum for a Day Ionosphere; Radial B_o = .4 Gauss

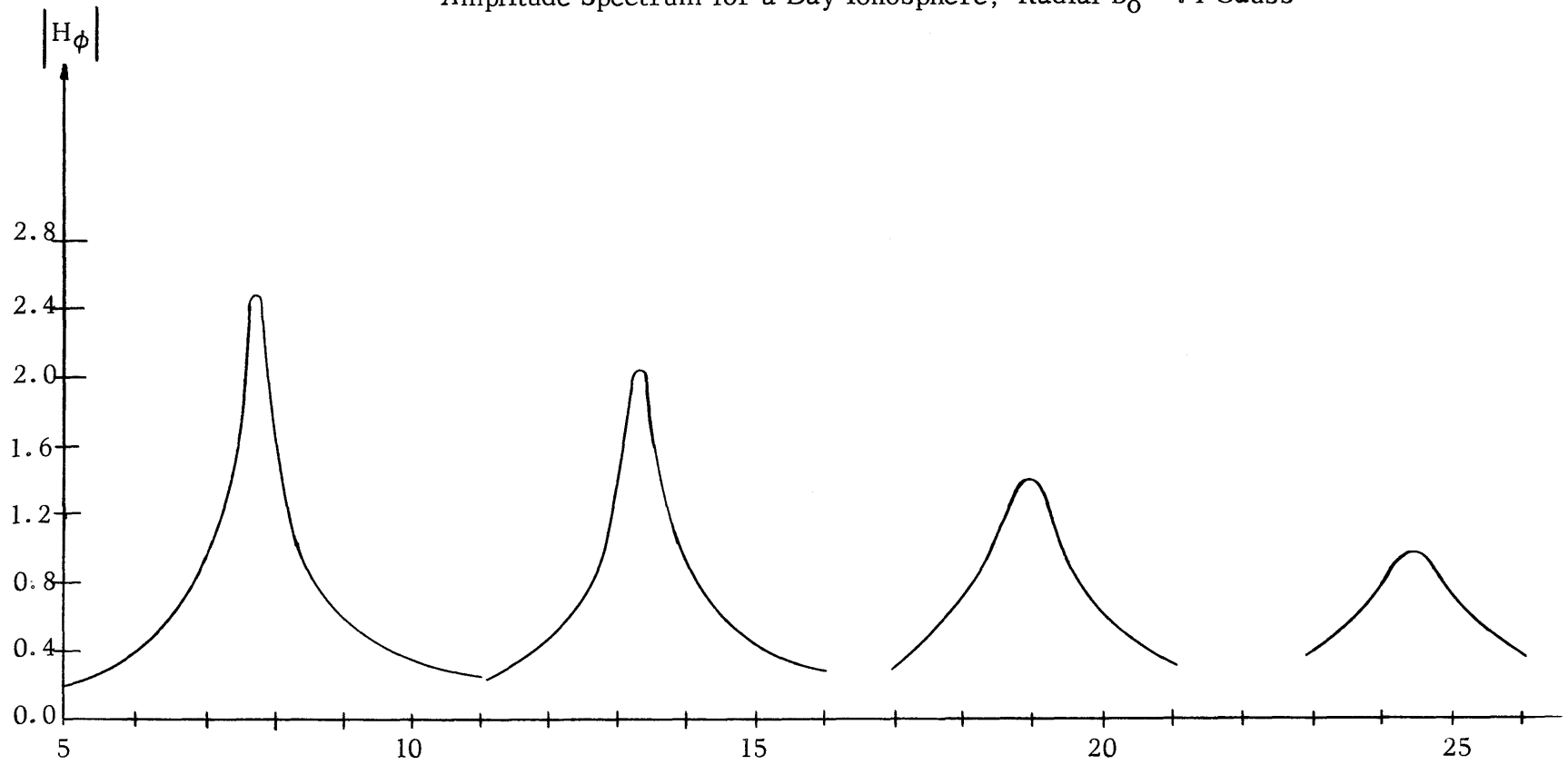

Figure 15

Amplitude Spectrum for a Day Ionosphere; Radial $B_o = 10^{-4}$ Gauss

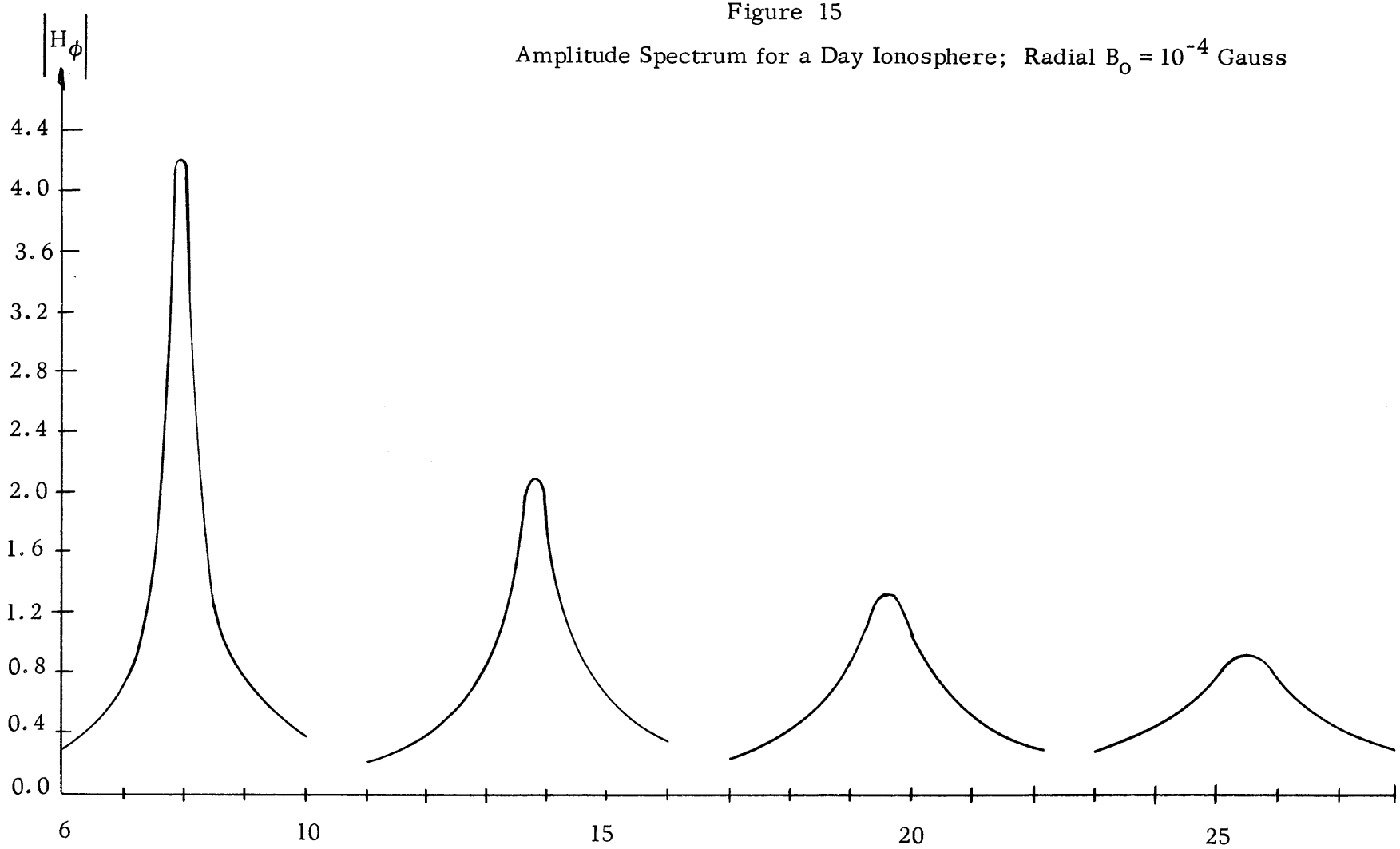

Figure 16

Amplitude Spectrum for the Night Ionosphere: Radial B_o = .4 Gauss

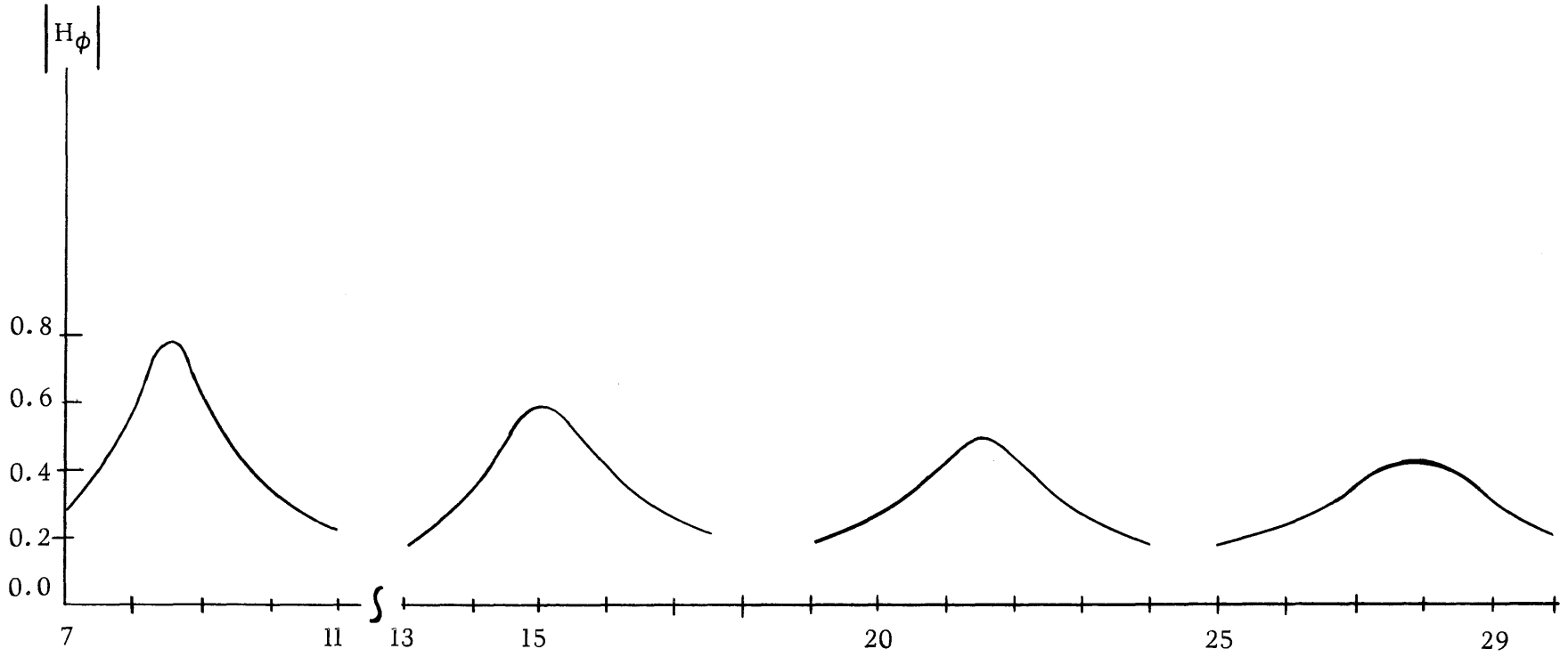

Figure 17

Amplitude Spectrum for the Night Ionosphere; Radial $B_0 = 10^{-4}$ Gauss

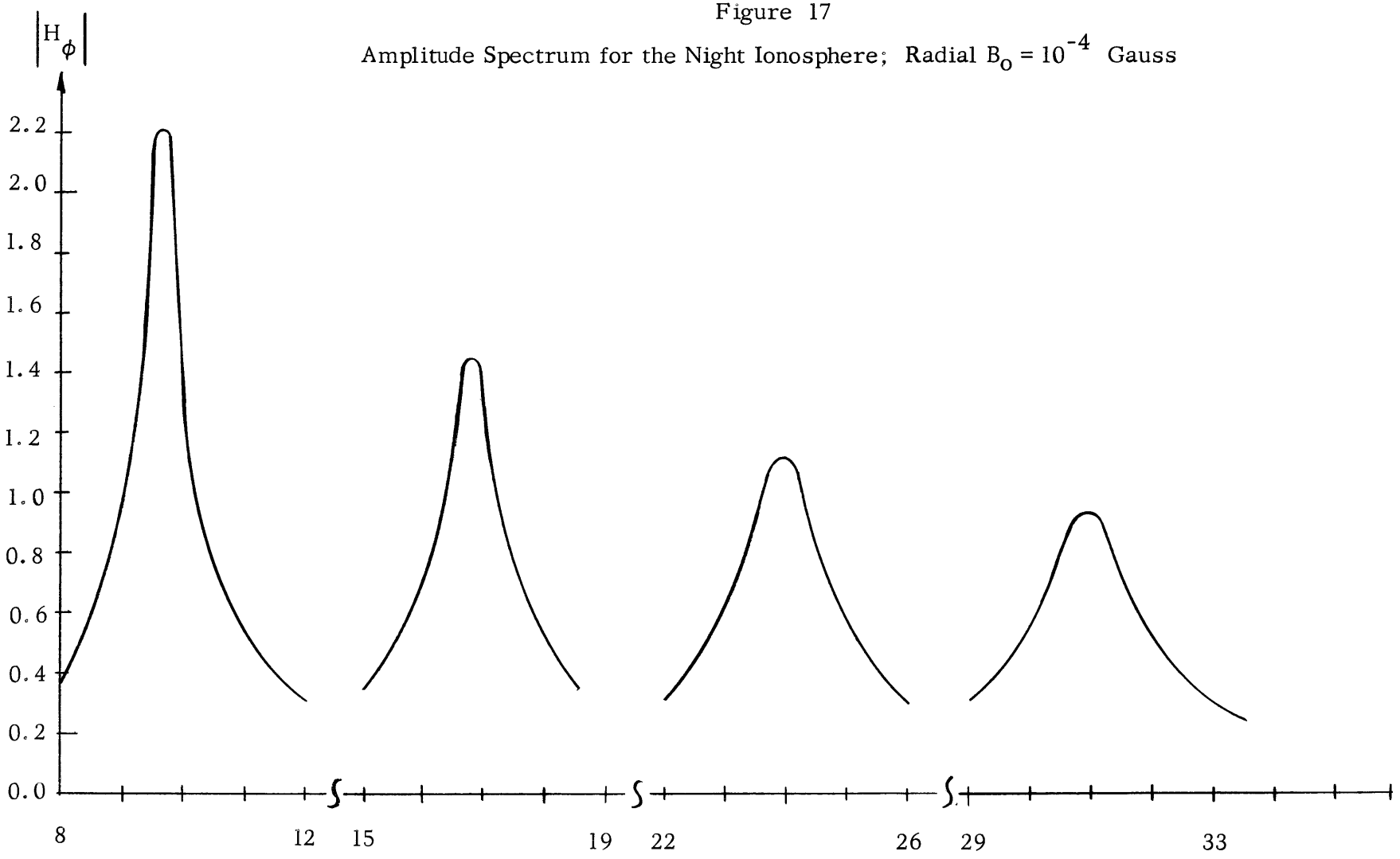

Figure 18

Model Fit to Daytime Electron Density Profile

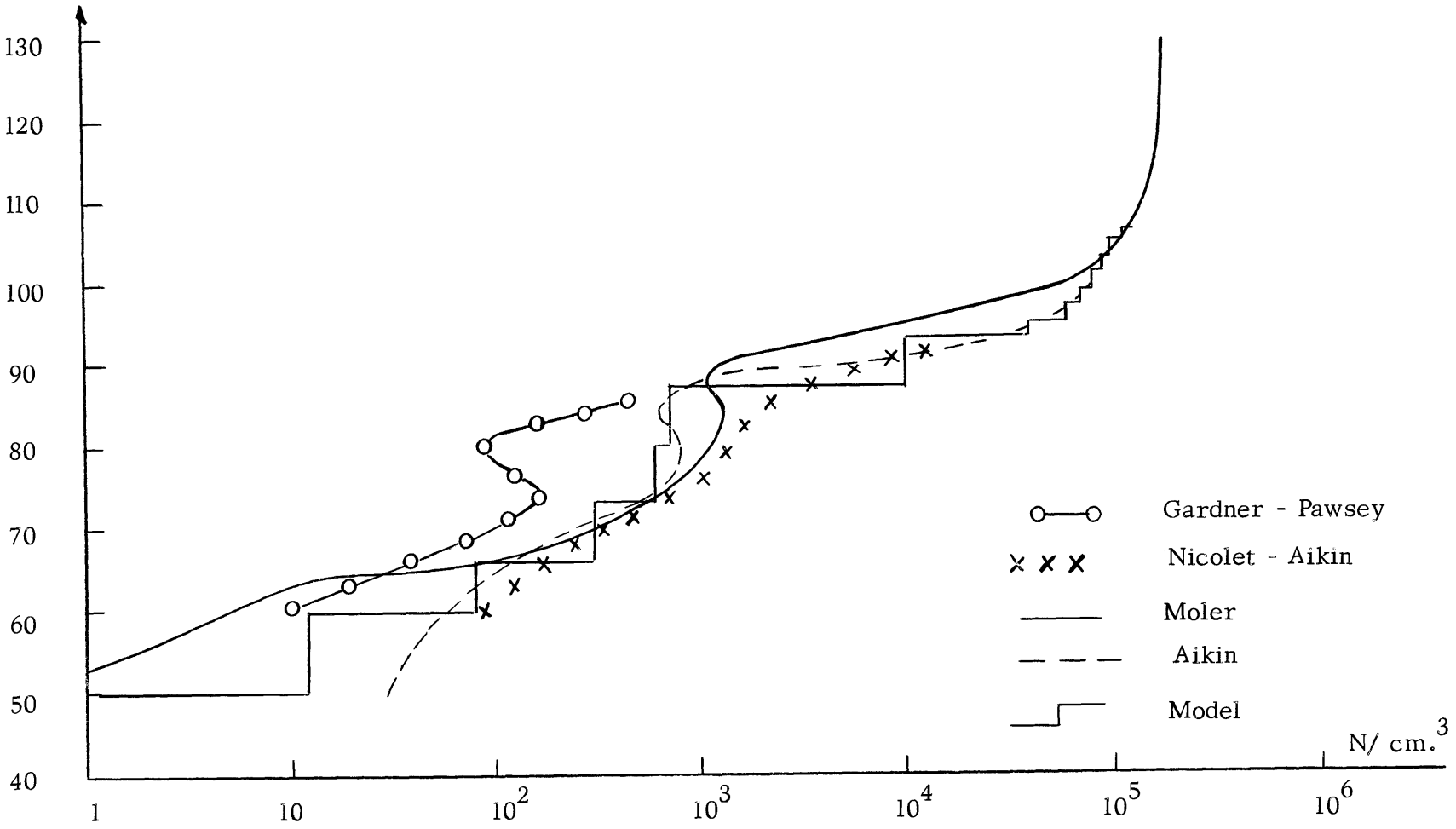

Figure 19

Daytime Electron and Ion Collision Frequencies

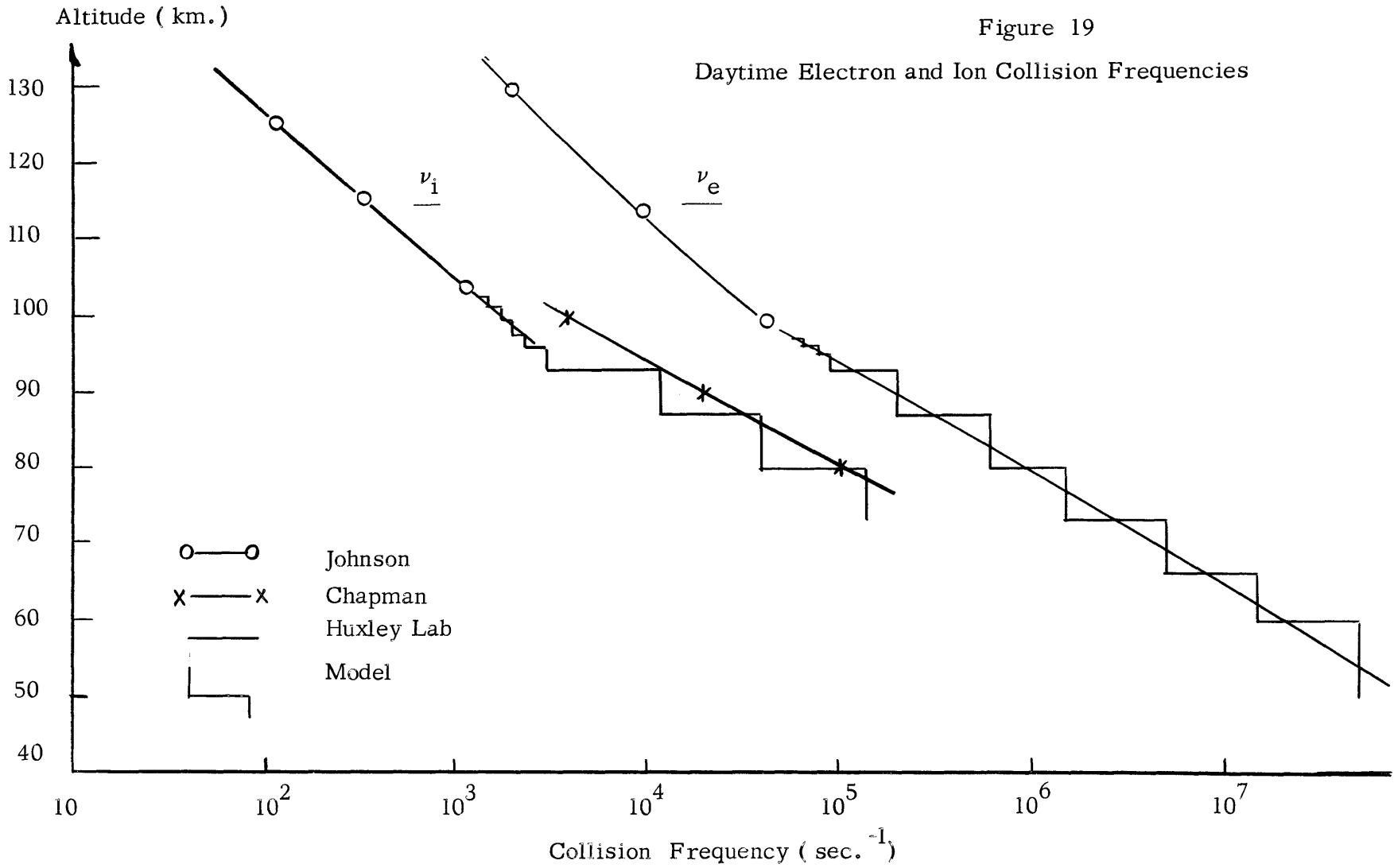

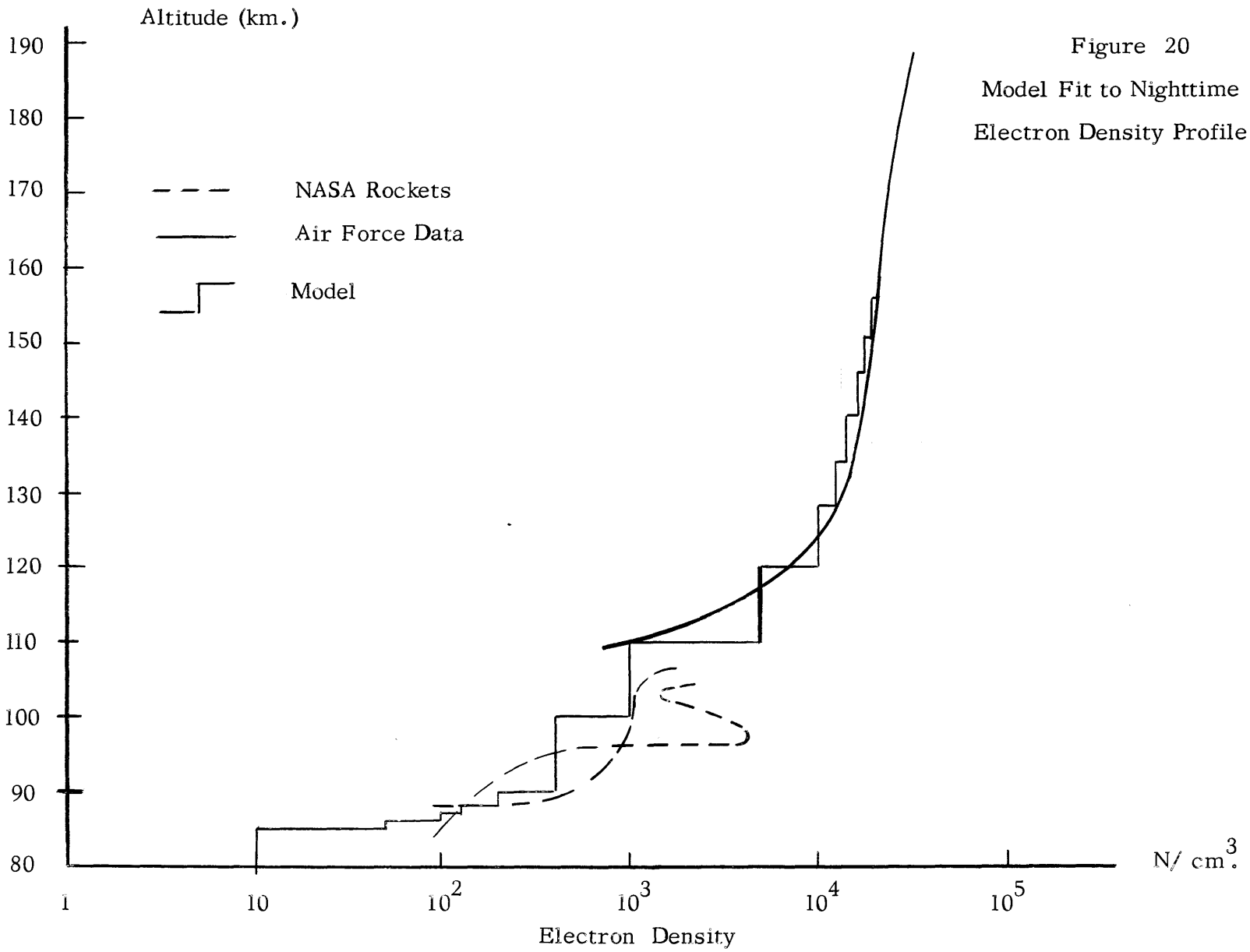

Figure 20

Model Fit to Nighttime

Electron Density Profile

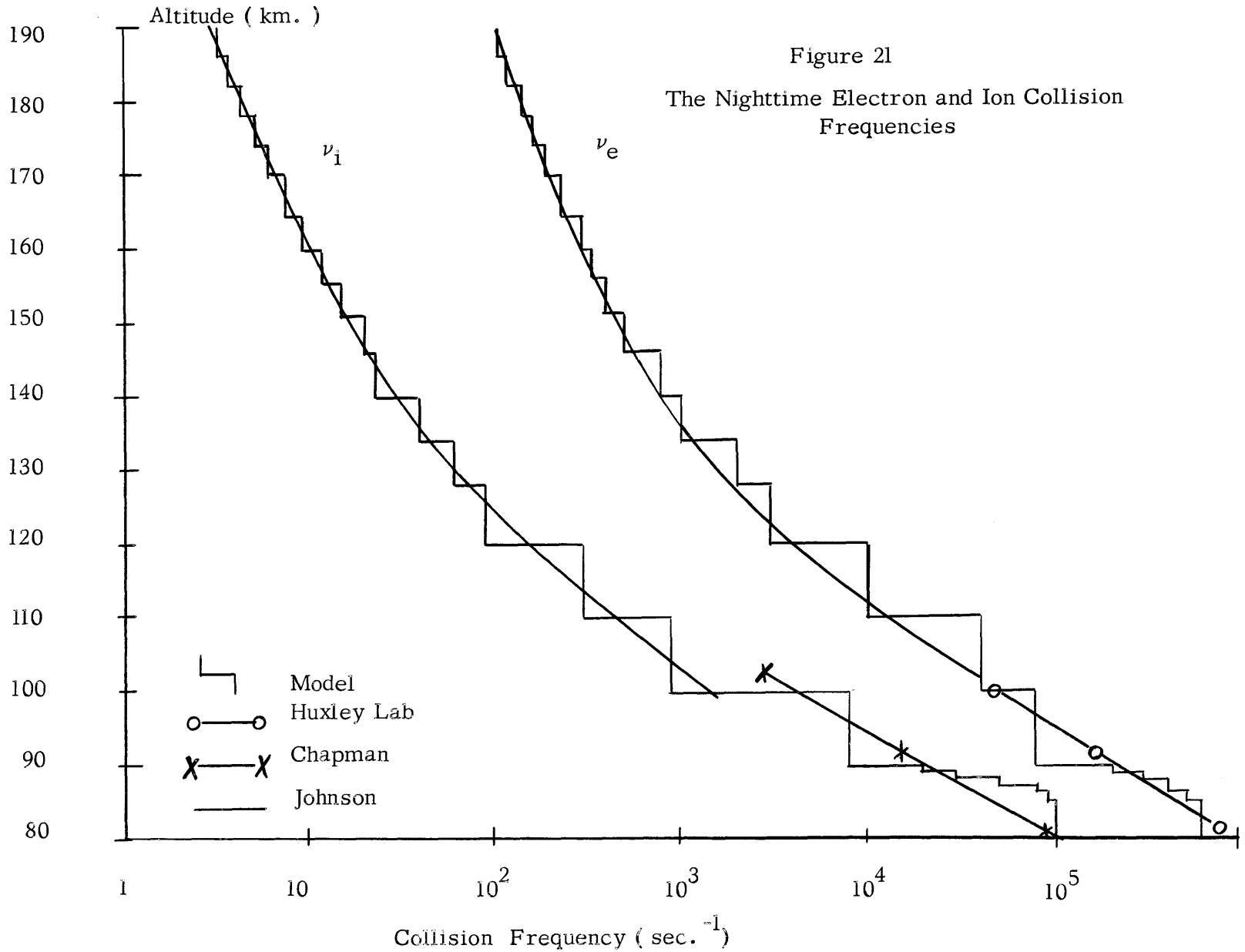

Figure 21

The Nighttime Electron and Ion Collision Frequencies

Concluding Remarks

One consistent observation which has not yet been discussed is the fact that the Q in the model results is always much higher than the experimental Q's of 4 to 6 measured by Balser and Wagner [1960]. Two features of the real cavity waves which could lower the measured Q are time variations in cavity properties and the asymmetry due to the geomagnetic field.

Short term variations of the mode structure which are averaged in time can only lower the experimental Q relative to the instantaneous Q, which is what the model measures. Balser and Wagner [1962] have shown that there are diurnal peak frequency drifts on the order of half a cycle. Their measurements are generally based on the statistical analysis of 3 minute real-time samples of the cavity noise. Unfortunately any attempt to observe the cavity properties for a much shorter time decreases the statistical reliability of the analysis.

The model has treated a symmetrical cavity with the source at $\theta = 0$. This allowed a spherical harmonic description which excluded the longitudinal dependence. In the real cavity the combination of the geomagnetic field and the sun effect an asymmetry for a source at any position that can only be described by the associated Legendre polynomials in the harmonic analysis. With this description the n^{th} mode consists of $2n+1$ waves which have different angular dependence and may therefore have slightly different peak frequencies. The model only considers the lowest order wave in each $2n+1$ set. Experimentally the summation of all the waves is observed. This can only lower the Q of a mode consisting of a single wave.

Suggestions for Further Work

Several complicating factors dealt with rather lightly here require further investigation if we are to fully understand the cavity properties.

One problem is that of incorporating into the model the non-radial conductivity changes. Real cavity effects of the day-night ionosphere, as an example, might be attacked by a relaxation technique in a two-dimensional cavity model in which the homogeneous layers were divided into sectors. This solution would give more realistic frequencies for the day-night cavity, as opposed to the method of computing the response due to average cavity properties, or using the average of the day and night model frequencies.

It would seem advantageous to pursue the cylindrical cavity model further and examine the problem of propagation in an anisotropic medium at an arbitrary angle to the geomagnetic field. This would give a quantitative estimate of how the cavity response changes in the region between purely longitudinal and transverse propagation.

Several avenues of investigation have been opened by recent experimental evidence. Balser and Wagner [1962] have presented a detailed analysis on the diurnal frequency variations of the first four modes which as yet has not yielded to a satisfactory explanation. Sudden conductivity disturbances caused by such phenomena as cosmic ray bursts from the sun and high altitude nuclear detonations may be treated as perturbation effects to determine their influence on the cavity properties.

Revised estimates of the conductivity parameters of the D layer, with emphasis on the ion composition, may warrant new calculations in the present model. Ion density profiles may be in error by one or two orders of magnitude in this region, and the lack of conclusive experimental data leaves something to be desired in this zone.

Summary of Data:

a. Daytime Electron Density

Gardner-Pawsey
Aikin — see Bourdeau [1962]
Nicolet and Aikin, see Reference [1960]
Moler, See Ref. [1960]
Profile above 100 km, see "Handbook of Geophysics," [1960]

b. Daytime Collision Frequencies

Johnson, see Ref. [1961]
Chapman, see Ref. [1956]
Huxley Lab., see Ref. [1953]

c. Nighttime Electron Density

NASA Rockets, see Bourdeau [1962]
Air Force Data, see "Handbook of Geophysics," [1960]

d. Nighttime Collision Frequencies

Same references as in (b).

LIST OF SYMBOLS

e = electron charge (taken as a positive quantity).

ν = collision frequency in $\sec^{-1}$.

ω = angular frequency of electromagnetic wave in rad/sec.

k_o = propagation constant in free space

$m_{e,i}$ = mass of electron, ion

$\omega_H = \frac{eB}{m_e}$ = electron gyrofrequency

$\Omega_H = \frac{eB}{m_i}$ = ion (single charge) gyrofrequency

μ = magnetic permittivity of free space

σ = conductivity in $(\text{ohm-meters})^{-1}$

B_o = geomagnetic field strength

E = electric field vector

H = magnetic field vector

APPENDIX I. Solution of the Equations of Motion of the Plasma for the Conductivity Tensor

In addition to the definitions in Section 1.3 the following terms are defined:

Plasma density $\rho_p = N_i m_i + N_e m_e = N_p m$ A.1.1

Neutral density $\rho_n = N_n m_n$ A.1.2

Plasma momentum $\rho_p \vec{v}_p = N_i m_i \vec{v}_i + N_e m_e \vec{v}_e$ A.1.3

Plasma velocity $= \vec{v}_p$

Since $N_i = N_e = N_p$, $\rho_p \vec{v}_p = N_p (m_i \vec{v}_i + m_e \vec{v}_e)$ A.1.4

and $\vec{J} = e N_p (\vec{v}_i - \vec{v}_e)$ A.1.5

We assume $m_n \sim m_i$

Solving (A.1.4) and (A.1.5) for $\vec{v}_i$ and $\vec{v}_e$,

$$\vec{v}_i = \vec{v}_p + b\vec{J} \qquad \text{A.1.6}$$

$$\vec{v}_e = \vec{v}_p - \frac{m_i}{m_e} b\vec{J} \qquad \text{A.1.7}$$

where $b = m_e / N_p e (m_e + m_i)$

Using $\frac{\partial}{\partial t} = -i\omega$ and adding Equations (1.3.2) and 1.3.3)

$$-i\omega \rho_p \vec{v}_p + N_p \nu_{en} m_e \left(\vec{v}_p - \frac{m_i}{m_e} b\vec{J} - \vec{v}_n \right) \qquad \text{A.1.8}$$

$$+ N_p \nu_{in} m_i (\vec{v}_p + b\vec{J} - \vec{v}_n) = \overrightarrow{J \times B}$$

Multiplying (1.3.2) by m_i and (1.3.3) by m_e and subtracting

$$i\omega\, m_i\, m_e\, \frac{\vec{J}}{e} - m_i\, m_e\, \nu_{ie}\, \frac{\vec{J}}{e} + N_p\, m_i\, m_e\, \vec{v}_p\, (\nu_{en} - \nu_{in})$$

$$- N_p\, m_i\, b\, \vec{J}\, (\nu_{en}\, m_i + \nu_{in}\, m_e) - \vec{v}_n\, N_p\, m_i\, m_e\, (\nu_{en} - \nu_{in})$$

$$= - e\, N_p\, \vec{E}\, (m_i + m_e) - e\, N_p\, (m_i + m_e)\, \vec{v}_p \times \vec{B} + e\, N_p\, b\, (\vec{J} \times \vec{B})\, \frac{m_i^2}{m_e} \qquad \text{A.1.9}$$

Using (A.1.6) and (A.1.7) Equation (1.3.1) can be solved for v_n.

$$\vec{v}_n = \alpha\, \vec{v}_p + \beta\, \vec{J} \qquad \text{A.1.10}$$

$$\text{where } \alpha = \frac{N_p\, (m_e\, \nu_{en} + m_i\, \nu_{in})}{N_p\, (m_e\, \nu_{en} + m_i\, \nu_{in}) - i\omega\rho_n}$$

$$\beta = \frac{N_p\, m_i\, b\, (\nu_{in} - \nu_{en})}{N_p\, (m_i\, \nu_{in} + m_e\, \nu_{en}) - i\omega\rho_n}$$

Substituting (A.1.10) into (A.1.8) and solving for v_p

$$\vec{v}_p = \Theta\, \vec{J} + \Psi\, (\vec{J} \times \vec{B}) \qquad \text{A.1.11}$$

$$\text{where } \Theta = \frac{N_p\, \nu_{en}\, m_e \left(\frac{m_i}{m_e}\, b + \beta\right) + N_p\, \nu_{in}\, m_i\, (-b + \beta)}{-i\omega\rho_p + N_p\, (\nu_{en}\, m_e + \nu_{in}\, m_i)\, (1 - \alpha)}$$

$$\Psi = \frac{1}{-i\omega\rho_p + N_p\, (\nu_{en}\, m_e + \nu_{in}\, m_i)\, (1 - \alpha)}$$

Now substituting (A.1.11) and (A.1.10) into (A.1.9),

$$c_0\, \vec{J} + c_1\, \vec{J} \times \vec{B} + c_2\, (\vec{J} \times \vec{B}) \times \vec{B} = - e\, N_p\, m\, \vec{E} \qquad \text{A.1.12}$$

where

$$c_0 = \frac{m_i\, m_e}{e}\, (i\omega - \nu_{ie}) + N_p\, m_i\, m_e\, (\nu_{en} - \nu_{in})\, \Theta$$

$$- N_p\, m_i\, b\, (\nu_{en}\, m_i + \nu_{in}\, m_e) - \beta\, N_p\, m_i\, m_e\, (\nu_{en} - \nu_{in}) - \alpha\, \Theta N_p m_i m_e\, (\nu_{en} - \nu_{in})$$

$$c_1 = N_p m_i m_e (\nu_{en} - \nu_{in}) \Psi - \alpha \Psi N_p m_i m_e (\nu_{en} - \nu_{in})$$

$$- e N_p b \frac{m_i^2}{m_e} + e N_p m \Theta$$

$$c_2 = e N_p m \Psi$$

In the altitude range up to 200 km. for a typical day ionosphere [Johnson, 1961]

Altitude	ν_{en}	ν_{in}	$\frac{m_i}{m_e} \nu_{in}$	Ion
100 km.	$4 \cdot 10^4$	$2 \cdot 10^3$	$11 \cdot 10^7$	NO^+
150 km.	$2 \cdot 10^3$	20	$11 \cdot 10^5$	NO^+
200 km.	$7 \cdot 10^2$	2	$11 \cdot 10^4$	NO^+
200 km.	$7 \cdot 10^2$	2	$6 \cdot 10^4$	O^+

Therefore, at least below 200 km. $m_i \nu_{in} \gg m_e \nu_{en}$. A.1.13

Using data of Francis and Karplus [1960], p. 3597, Table 4, and Johnson [1961] at a frequency of $\omega = 100$ rad. sec.$^{-1}$, again for a day ionosphere,

Altitude	N_n	ω	N_p	ν_{in}
100 km.	10^{13}	10^2	10^5	$2 \cdot 10^3$
160 km.	$5 \cdot 10^{10}$	10^2	$3 \cdot 10^5$	20
200 km.	10^{10}	10^2	$3 \cdot 10^5$	2

Therefore a valid approximation in this region is $N_n \omega \gg N_p \nu_{in}$. But since $m_i \cong m_n$, $\rho_n \omega \gg N_p m_i \nu_{in}$.

It has been shown in (A.1.13) that $m_i \nu_{in} \gg m_e \nu_{en}$, so

$$\rho_n \omega \gg N_p (m_i \nu_{in} + m_e \nu_{en}) \qquad \text{A.1.14}$$

Using the approximations (A. 1. 13) and (A. 1. 14) reduces the complexity of the coefficients.

$$\alpha \cong \frac{N_p \nu_{in}}{-i\omega N_n} \ll 1$$

$$\beta \cong \frac{m_e}{em} \frac{(\nu_{in} - \nu_{en})}{-i\omega N_n}$$

$$\Theta \cong \frac{m_e}{N_p em} \frac{\nu_{en} - \nu_{in}}{\nu_{in} - i\omega}$$

$$\Psi \cong \frac{1}{N_p m_i (\nu_{in} - i\omega)}$$

Applying the above definitions in conjunction with (A. 1. 13) and (A. 1. 14), and recalling that at these altitudes $m_i > 10^4 m_e$,

$$c_0 = \frac{m_i m_e}{e} (i\omega - \nu_{ie} - \nu_{en})$$

$$c_1 = - m_i$$

$$c_2 = \frac{e}{\nu_{in} - i\omega}$$

Equation (A. 1. 12) becomes, using these expressions for c_0, c_1, and c_2,

$$\vec{J} \frac{m_i m_e}{e} (i\omega - \nu_{ie} - \nu_{en}) - m_i \overrightarrow{(J \times B)}$$

$$+ \frac{e}{\nu_{in} - i\omega} \overrightarrow{(J \times B) \times B} = -e N_p m \vec{E}$$

To solve this equation for the resistivity tensor in spherical coordinates,

$$\overrightarrow{J \times B} = \hat{r} (J_\theta B_\phi - J_\phi B_\theta) + \hat{\theta} (J_\phi B_r - J_r B_\phi)$$

$$+ \hat{\phi} (J_r B_\theta - J_\theta B_r)$$

$$\overrightarrow{(J \times B) \times B} = \hat{r}\,[B_\phi (J_\phi B_r - J_r B_\phi) - B_\theta (J_r B_\theta - J_\theta B_r)]$$

$$+ \hat{\theta}\,[B_r (J_r B_\theta - J_\theta B_r) - B_\phi (J_\theta B_\phi - J_\phi B_\theta)]$$

$$+ \hat{\phi}\,[B_\theta (J_\theta B_\phi - J_\phi B_\theta) - B_r (J_\phi B_r - J_r B_\phi)]$$

With the notation

$$x = \frac{m_e}{N_p e^2}(\nu_e - i\omega)$$

$$\nu_e = \nu_{ei} + \nu_{en} \qquad y = \frac{1}{N_p e}$$

$$z = \frac{1}{N_p m (\nu_{in} - i\omega)}$$

equation (A.1.12) becomes

$$\vec{E} = x\vec{J} + y\,\overrightarrow{(J \times B)} - z\,\overrightarrow{(J \times B) \times B} \qquad \text{(A.1.15)}$$

When $B_r = B_0$, $B_\theta = B_\phi = 0$, (A.1.15) becomes

$$\begin{bmatrix} E_r \\ E_\theta \\ E_\phi \end{bmatrix} = \begin{bmatrix} x & 0 & 0 \\ 0 & x + B_0^2 z & yB_0 \\ 0 & -yB_0 & x + B_0^2 z \end{bmatrix} \cdot \begin{bmatrix} J_r \\ J_\theta \\ J_\phi \end{bmatrix}$$

OR, $E_i = R_{ij} J_j$

$$R_{ij}^{-1} = \sigma_{ij} = \begin{bmatrix} \frac{1}{x} & 0 & 0 \\ 0 & \frac{x + B_0^2 z}{(x + B_0^2 z)^2 + y^2 B_0^2} & \frac{-yB_0}{(x + B_0^2 z)^2 + y^2 B_0^2} \\ 0 & \frac{yB_0}{(x + B_0^2 z)^2 + y^2 B_0^2} & \frac{x + B_0^2 z}{(x + B_0^2 z)^2 + y^2 B_0^2} \end{bmatrix}$$

Let $\sigma_{11} = \frac{1}{x} = \frac{Ne^2}{m_e} \frac{1}{(\nu_e - i\omega)}$

Since $m_e (\nu_e - i\omega) \ll m_i (\nu_i - i\omega)$ σ_{11} only has a contribution from the electrons.

Let $\sigma_\perp = \frac{x + B_0^2 z}{(x+B_0^2 z)^2 + y^2 B_0^2}$

Again using the approximation that $m_i (\nu_i - i\omega) \gg m_e (\nu_e - i\omega)$, where $\nu_i = \nu_{in}$, which was used in the derivation of the resitivity tensor, this is equal to the definition of

$$\sigma_\perp = Ne^2 \left[\frac{\nu_e - i\omega}{m_e [(\nu_e - i\omega)^2 + \omega_H^2]} + \frac{\nu_i - i\omega}{m_i [(\nu_i - i\omega)^2 + \Omega_H^2]} \right]$$

as given by Johnson [1961] when the same approximation is applied.

Similarly if $\sigma_x = \frac{-y B_0}{(x+B_0^2 z)^2 + y^2 B_0^2}$ this is equivalent to

$$\sigma_x = Ne^2 \left[\frac{-\omega_H}{m_e [(\nu_e - i\omega)^2 + \omega_H^2]} + \frac{\Omega_H}{m_i [(\nu_i - i\omega)^2 + \Omega_H^2]} \right]$$

The derivation of the resistivity tensor for the two remaining geomagnetic orientations, namely $B_\Theta = B_0$ and $B_\phi = B_0$, follow in a manner analogous to the case when $B_r = B_0$.

APPENDIX II. The Wave Solutions for Anisotropic Media

A. Cylindrical Coordinates, Geomagnetic Field in the $\hat{z}$ Direction

The conductivity tensor, given by (1.3.14), (where cylindrical $\hat{z}$ takes the place of spherical $\hat{\phi}$) is

$$\sigma_{ij} = \begin{vmatrix} \sigma_\perp & \sigma_x & 0 \\ -\sigma_x & \sigma_\perp & 0 \\ 0 & 0 & \sigma_{11} \end{vmatrix}$$

The two vector equations (2.1.1) and (2.1.2), when written out in each of their three components, yield six partial differential equations composed of two independent sets of three equations each.

One of these sets is the TE mode and involves the vectors E_r, E_θ, and H_z as follows:

$$\frac{\partial E_\theta}{\partial r} + \frac{E_\theta}{r} - \frac{1}{r}\frac{\partial E_r}{\partial \theta} = i\mu\omega H_z \qquad \text{A.2.1}$$

$$\frac{1}{r}\frac{\partial H_z}{\partial \theta} = \sigma_\perp E_r + \sigma_x E_\theta \qquad \text{A.2.2}$$

$$-\frac{\partial H_z}{\partial r} = -\sigma_x E_r + \sigma_\perp E_\theta \qquad \text{A.2.3}$$

Using $\frac{\partial}{\partial \theta} = in$, the above equations may be solved simultaneously for any one of the vectors. Choosing H_z results in a partial differential equation (where prime indicates $\frac{\partial}{\partial r}$)

$$H_z'' + \frac{H_z'}{r} + H_z \left[-\frac{n^2}{r^2} + k_\perp^2 - \left(\frac{u\omega\sigma_x}{k_\perp}\right)^2 \right] = 0 \qquad \text{A.2.4}$$

which is recognized as Bessel's Equation.

The solution of (A.2.4) applicable here is

$$H_z = a_n H_n(k_p r), \quad k_p^2 = k_\perp^2 + \frac{k_x^4}{k_\perp^2} \qquad \text{A.2.5}$$

where H_n is a Hankel function of order n.

Solving for the remaining components

$$E_r = \frac{a_n \mu\omega}{k_\perp^4 + k_x^4} \left[-\mu\omega\sigma_x H_n'(k_p r) - k_\perp^2 \frac{n}{r} H_n(k_p r) \right] \qquad \text{A.2.6}$$

$$E = \frac{a_n i\mu\omega}{k_\perp^4 + k_x^4} \left[-\mu\omega\sigma_x \frac{n}{r} H_n(k_p r) - k_\perp^2 H_n'(k_p r) \right] \qquad \text{A.2.7}$$

The time and angular dependence will not be repeated; all vectors have the same $\exp(in\theta - i\omega t)$ factor. It is understood that there are solutions $H_n^{(1)}$ for the outgoing wave and $H_n^{(2)}$ for the incoming wave.

The other set of three partial differential equations contains the vectors H_r, H_θ, and E_z and describes the TM mode.

$$\frac{1}{r} \frac{\partial E_z}{\partial \theta} = i\mu\omega H_r \qquad \text{A.2.8}$$

$$-\frac{\partial E_z}{\partial r} = i\mu\omega H_\theta \qquad \text{A.2.9}$$

$$\frac{\partial H_\theta}{\partial r} + \frac{H_\theta}{r} - \frac{1}{r} \frac{\partial H_r}{\partial \theta} = \sigma_{11} E_z \qquad \text{A.2.10}$$

Notice that this set does not contain $\sigma_\perp$ or σ_x and hence is a mode of propagation unaffected by the magnetic field.

Solution of these three equations gives the known TM mode for isotropic media

$$\text{(a)} \quad E_z = b_n H_n(k_{11} r)$$

$$\text{(b)} \quad H_r = b_n \frac{n}{\mu\omega r} H_n(k_{11} r) \qquad \text{A.2.11}$$

$$\text{(c)} \quad H_\theta = b_n \frac{i}{\mu\omega} H_n'(k_{11} r)$$

The TM mode has its only electric field vector parallel to the geomagnetic field, so $\bar{v} \times \bar{B}$ terms in the equations of motion are zero.

B. Cylindrical Coordinates, Geomagnetic Field in the $\hat{\theta}$ Direction

The conductivity tensor is given by (1.3.12)

$$\sigma_{ij} = \begin{vmatrix} \sigma_\perp & 0 & -\sigma_x \\ 0 & \sigma_{11} & 0 \\ \sigma_x & 0 & \sigma_\perp \end{vmatrix}$$

Separating the Maxwell equations with this definition of σ_{ij}

$$\text{(a)} \quad \frac{1}{r} \frac{\partial E_z}{\partial \theta} = i\mu\omega H_r$$

$$\text{(b)} \quad -\frac{\partial E_z}{\partial r} = i\mu\omega H_\theta$$

$$\text{(c)} \quad \frac{\partial E_\theta}{\partial r} + \frac{E_\theta}{r} - \frac{1}{r} \frac{\partial E_r}{\partial \theta} = i\mu\omega H_z$$

B.2.1

$$\text{(d)} \quad \frac{1}{r} \frac{\partial H_z}{\partial \theta} = \sigma_\perp E_r - \sigma_x E_z$$

$$\text{(e)} \quad -\frac{\partial H_z}{\partial r} = \sigma_{11} E_\theta$$

$$\text{(f)} \quad \frac{\partial H_\theta}{\partial r} + \frac{H_\theta}{r} - \frac{1}{r} \frac{\partial H_r}{\partial \theta} = \sigma_x E_r + \sigma_\perp E_z$$

The terms containing σ_x couple the six equations in (B.2.1) so they may not be separated into two independent sets as when $B_z = B_0$. There will still be two modes of propagation, but now each mode will contain all six components of E and H.

Simultaneous solution of Equations (B.2.1) for $E_z(r)$ results in the fourth order differential equation

$$E_z'''' + \frac{4}{r} E_z''' + E_z'' (k_{11}^2 + k_p^2) + \frac{E_z'}{r} (k_{11}^2 + 3k_p^2)$$

$$+ E_z (k_{11}^2 k_p^2) = 0 \qquad \text{B.2.2}$$

where $k_p^2 = k_\perp^2 + \frac{k_x^4}{k_\perp^2}$

The approximation $k_\perp^2 r^2 \gg n^2$ has been made in the derivation of (B.2.2); this is justified at the close of Section 2.2

The solution of (B.2.2) is

$$E_z = \frac{a_n e^{\pm i k_p r}}{r^{1/2}} \qquad \text{B.2.3}$$

and $$E_z = b_n \frac{e^{\pm i k_{11} r}}{r^{3/2}} \qquad \text{B.2.4}$$

Once E_z is known the remaining components of E and H by substituting back into Equations (B.2.1)

For the k_p mode

$$\text{(a)} \quad E_r = a_n \frac{e^{ik_p r}}{r^{1/2}} \frac{\sigma_x}{\sigma_\perp}$$

$$\text{(b)} \quad E_\theta = a_n \frac{e^{ik_p r}}{r^{3/2}} \frac{n k_p \sigma_x}{\sigma (k_p^2 - k^2{}_{11})}$$

$$\text{(c)} \quad E_z = a_n \frac{e^{ik_p r}}{r^{1/2}}$$

$$\text{(d)} \quad H_r = \frac{a_n n e^{ik_p r}}{u\omega r^{3/2}} \qquad \text{B.2.5}$$

$$\text{(e)} \quad H_\theta = -\frac{1}{i\mu\omega} \frac{a_n e^{ik_p r}}{r^{1/2}} \left(ik_p - \frac{1}{2r}\right)$$

$$(f)\quad H_z = i\,\frac{a_n e^{ik_p r}}{r^{3/2}}\quad \frac{n\,\sigma_{11}\,\sigma_x}{\sigma\,(k_p^2 - k_{11}^2)}$$

Notice that for $B_\theta \rightarrow 0$, $k_p \rightarrow k = k_{11}$ and $\sigma_x \rightarrow 0$. Therefore in Equations (B.2.5) E_r, E_θ, $H_z \rightarrow 0$ and only the TM mode remains. $\sigma_x/(\sigma_p - \sigma_{11})$ goes to zero as the geomagnetic field goes to zero for conductivities which include both electrons and ions.

For the k_{11} mode the vector solutions are

$$(a)\quad E_r = n\,b_n\,\frac{e^{ik_{11}r}}{r^{3/2}}\quad \frac{\sigma_{11} - \sigma}{\sigma_{11} - \sigma_p}$$

$$(b)\quad E_\theta = -\frac{\sigma}{\sigma_{11}}\quad \frac{b_n\, e^{ik_{11}r}}{r^{1/2}}\quad \left(k_{11} + \frac{i}{2r}\right)$$

$$(c)\quad E_z = \frac{b_n\, e^{ik_{11}r}}{r^{3/2}}\quad \frac{n\sigma_x}{\sigma_{11} - \sigma_p}$$

B.2.6

$$(d)\quad H_r = b_n\,\frac{n^2\,\sigma_x}{\mu\,\omega}\quad \frac{e^{ik_{11}r}}{r^{5/2}}\quad \frac{1}{\sigma_{11} - \sigma_p}$$

$$(e)\quad H_\theta = -k_{11}\,\frac{n\,\sigma_x}{\mu\,\omega}\quad \frac{b_n\, e^{ik_{11}r}}{r^{3/2}}\quad \frac{1}{\sigma_{11} - \sigma_p}$$

$$(f)\quad H_z = -i\,b_n\,\frac{e^{ik_{11}r}}{r^{1/2}}\quad \sigma$$

As before, when $B_\theta \rightarrow 0$, $\sigma_x/(\sigma_p - \sigma_{11}) \rightarrow 0$ and E_z, H_r, $H_\theta \rightarrow 0$. In this case of isotropic propagation only the TE mode (E_r, E_θ, H_z) remains.

C. Cylindrical Coordinates, Geomagnetic Field in the $\hat{r}$ Direction

The conductivity tensor from (1.3.10) is

$$\sigma_{ij} = \begin{matrix} \sigma_{11} & 0 & 0 \\ 0 & \sigma & \sigma_x \\ 0 & -\sigma_x & \sigma \end{matrix}$$

and the Maxwell equations are expressed as

$$\text{(a)}\quad \frac{1}{r}\frac{\partial E_z}{\partial \theta} = i\mu\omega H_r$$

$$\text{(b)}\quad -\frac{\partial E_z}{\partial r} = i\mu\omega H_\theta$$

$$\text{(c)}\quad \frac{\partial E_\theta}{\partial r} + \frac{E_\theta}{r} - \frac{1}{r}\frac{\partial E_r}{\partial \theta} = i\mu\omega H_z$$

C.2.1

$$\text{(d)}\quad \frac{1}{r}\frac{\partial H_z}{\partial \theta} = \sigma_{11} E_r$$

$$\text{(e)}\quad -\frac{\partial H_z}{\partial r} = \sigma_\perp E_\theta + \sigma_x E_z$$

$$\text{(f)}\quad \frac{\partial H_\theta}{\partial r} + \frac{H_\theta}{r} - \frac{1}{r}\frac{\partial H_r}{\partial \theta} = -\sigma_x E_\theta + \sigma_\perp E_z$$

Again as in the case where $B_\theta = B_0$ the σ_x terms manage to couple equations (C.2.1) so that each of the two modes of propagation will contain all components of E and H.

Simultaneous solution of (C.2.1) for $E_z(r)$ results in the fourth order differential equation

$$E_z'''' + 2\frac{E_z'''}{r} + 2k_\perp^2 E_z'' + 2k_\perp^2\frac{E_z'}{r} + E_z\,(k_\perp^4 + k_x^4) = 0 \qquad \text{C.2.2}$$

where it has been assumed that $k_\perp^2 r^2 \gg n^2$ and $k_{11}^2 r^2 \gg n^2$.

The solution of (C.2.2) for the radial dependence of E_z is

$$E_z(r) = a_n \frac{e^{ikr}}{r^{1/2}}, \quad k^2 = k_\perp^2 \pm ik_x^2 \qquad \text{C.2.3}$$

where the ($\mp$) sign indicates the two different modes.

The solution for the remaining field components is

(a) $E_r = \mp \frac{a_n n e^{ikr}}{k_{11}^2 r^{3/2}} \quad (ik + \frac{1}{2r})$

(b) $E_\theta = \mp i \frac{a_n e^{ikr}}{r^{1/2}}$

(c) $E_z = a_n \frac{e^{ikr}}{r^{1/2}}$

C.2.4

(d) $H_r = \frac{n a_n e^{ikr}}{\mu \omega r^{3/2}}$

(e) $H_\theta = \frac{i a_n}{\mu \omega} \frac{e^{ikr}}{r^{1/2}} \quad (ik - \frac{1}{2r})$

(f) $H_z = \mp \frac{a_n e^{ikr}}{\mu \omega r^{1/2}} \quad (ik + \frac{1}{2r})$

D. Spherical Coordinates, Geomagnetic Field in the Radial Direction

The conductivity tensor applicable here is the same as in Section C for the cylindrical problem. When the Maxwell Equations (2.1.1) and (2.1.2) are written out in component form for anisotropic media, assuming the isotropic $\hat{\theta}$ dependence of (2.2.1), the results for the case of radial B field are

(a) $-n(n+1) \frac{H_\phi}{r} = \sigma_{11} E_r$

(b) $-\frac{1}{r} H_\phi - \frac{\partial H_\phi}{\partial r} = \sigma_x E_\phi + \sigma_\perp E_\theta$

(c) $\frac{\partial H_\theta}{\partial r} + \frac{H_\theta}{r} - \frac{H_r}{r} = -\sigma_x E_\theta + \sigma_\perp E_\phi$

$$\text{(d)} \quad -n(n+1)\frac{E_\phi}{r} = i\mu\omega H_r \qquad \text{D.2.1}$$

$$\text{(e)} \quad -\frac{\partial E_\phi}{\partial r} - \frac{E_\phi}{r} = i\mu\omega H_\theta$$

$$\text{(f)} \quad \frac{\partial E_\theta}{\partial r} + \frac{E_\theta}{r} - \frac{E_r}{r} = i\mu\omega H_\phi$$

where displacement currents have been neglected and $E_\phi = E_\phi(r)$, etc. The Legendre polynomials which appear as common factors in each of Equations (D.2.1) are the same as in the isotropic case.

Proceeding to solve Equations (D.2.1) simultaneously for E_r results in the fourth order differential equation

$$E_r'''' + \frac{8}{r}E_r''' + 2k_\perp^2 E_r'' + \frac{8}{r}k_\perp^2 E_r' + (k_\perp^4 + k_x^4)E_r = 0 \qquad \text{D.2.2}$$

where the approximation $k_\perp^2 r^2 \gg n(n+1)$ is made. The solution to (D.2.2) is

$$E_r = \frac{e^{ikr}}{r^2}, \text{ where } k^2 = k_\perp^2 \pm ik_x^2 \qquad \text{D.2.3}$$

where $(\pm)$ indicates the two possible modes.

Now using (D.2.3) to solve for the remaining field components, the radial dependent factors are given by

$$\text{(a)} \quad E_r = a_n\, n(n+1)\frac{e^{ikr}}{r^2}$$

$$\text{(b)} \quad E_\theta = a_n \frac{ik\, e^{ikr}}{r}\, \sigma_{11} \frac{(\sigma_\perp \mp i\sigma_x)}{(\sigma_\perp^2 + \sigma_x^2)}$$

$$\text{(c)} \quad E_\phi = a_n \frac{ik\, e^{ikr}}{r}\, \sigma_{11} \frac{(\sigma_x \pm i\sigma_\perp)}{(\sigma_\perp^2 + \sigma_x^2)}$$

(d) $$H_r = - a_n \frac{e^{ikr}}{r^2} \; n\,(n+1) \; \frac{k}{\mu\omega} \; \sigma_{11} \; \frac{(\sigma_x \pm i\,\sigma_\perp)}{(\sigma_x^2 + \sigma_\perp^2)}$$ D.2.4

(e) $$H_\theta = \pm\, i\, a_n \; \sigma_{11} \; \frac{e^{ikr}}{r}$$

(f) $$H_\phi = - a_n \, \sigma_{11} \; \frac{e^{ikr}}{r}$$

APPENDIX III. The Analytical Determination of $a_n(r_n)a_n^{-1}(r_{n+1})$ in Spherical Coordinates

The machine computation of the solution to the cavity problem for a large number of layers can be greatly accelerated if the analytical expression for the matrix $a_n(r_n)x\ a_n^{-1}(r_{n+1})$ is known. This is the matrix which expresses the solution at the top of the nth layer in terms of the solution at the bottom; ie, it expresses the influence of the nth layer on the wave passing through it. If the analytical expression for $a_n(r_n)a_n^{-1}(r_{n+1}) = d_n$ is known, it saves the computer one matrix inversion and one matrix product for each layer. Analytically there are only two different d_n's : one for the air layer, and a second for any layer in the ionosphere.

d_n for the air is an extremely useful expression because the Hankel functions which appear in the a_n's are absent, leaving the algebraic terms in the d_n matrix very easy to evaluate. This is due to the fact that we are dealing with a medium in which the radial thickness is very much less than a wavelength. The wave solutions in air are well known.

$$\text{Let} \quad S_n(r) = \begin{vmatrix} E_\theta \\ H_\phi \\ E_\phi \\ H_\theta \end{vmatrix} = a_n(r)\, c_n$$

$$\text{In air} \quad a_n(r) = \begin{vmatrix} a_{11} & a_{12} & 0 & 0 \\ a_{21} & a_{22} & 0 & 0 \\ 0 & 0 & a_{33} & a_{34} \\ 0 & 0 & a_{43} & a_{44} \end{vmatrix}$$

where, for r = a = radius of the earth, and $\sigma_o = k_o^2 / i\mu\omega$

$$a_{11} = \frac{1}{\sigma_o \sqrt{a}} \left[\frac{n}{a} H^{(1)}_{n+\frac{1}{2}}(k_o a) - k_o H^{(1)}_{n-\frac{1}{2}}(k_o a) \right]$$

$$a_{12} = \frac{1}{\sigma_o \sqrt{a}} \left[\frac{n}{a} H^{(2)}_{n+\frac{1}{2}}(k_o a) - k_o H^{(2)}_{n-\frac{1}{2}}(k_o a) \right]$$

$$a_{21} = \frac{1}{\sqrt{a}} H^{(1)}_{n+\frac{1}{2}}(k_o a) \qquad a_{22} = \frac{1}{\sqrt{a}} H^{(2)}_{n+\frac{1}{2}}(k_o a)$$

$$a_{33} = i\mu\omega\, a_{21} \qquad a_{34} = i\mu\omega\, a_{22}$$

$$a_{43} = \sigma_o a_{11} \qquad a_{44} = \sigma_o a_{12}$$

In this case $r_n = r_o = a$ and $r_{n+1} = r_1 = R = a + h$, where h is the air layer thickness.

Let $a_n(R) = [b_{ij}]$, where $b_{ij}(R) = a_{ij}(a)$ and $a_n^{-1}(R) = [c_{ij}] / |a_n(R)|$. $|a_n(R)|$ is the determinant of the matrix $[a_n(R)]$.

$$[c_{ij}] = \begin{vmatrix} c_{11} & c_{12} & 0 & 0 \\ c_{21} & c_{22} & 0 & 0 \\ 0 & 0 & c_{33} & c_{34} \\ 0 & 0 & c_{43} & c_{44} \end{vmatrix}$$

Let $x_1 = \frac{i\mu\omega}{R} k_o W(k_o R)$ and $x_2 = -x_1 / k_o^2$

where $W(k_o R) = H^{(2)}_{n+\frac{1}{2}}(k_o R) H^{(1)}_{n-\frac{1}{2}}(k_o R) - H^{(1)}_{n+\frac{1}{2}}(k_o R) H^{(2)}_{n-\frac{1}{2}}(k_o R)$ is the Bessel wronskian.

$$c_{11} = \frac{x_1}{\sqrt{R}} H^{(2)}_{n+\frac{1}{2}}(k_0 R) \qquad c_{12} = \frac{-x_1}{\sigma_o \sqrt{R}} \left[\frac{n}{R} H^{(2)}_{n+\frac{1}{2}}(k_o R) - k_o H^{(2)}_{n-\frac{1}{2}}(k_o R) \right]$$

$$c_{21} = \frac{-x_1}{\sqrt{R}} H^{(1)}_{n+\frac{1}{2}}(k_o R) \qquad c_{22} = \frac{x_1}{\sigma_o \sqrt{R}} \left[\frac{n}{R} H^{(1)}_{n+\frac{1}{2}}(k_o R) - k_o H^{(1)}_{n-\frac{1}{2}}(k_o R) \right]$$

$$c_{33} = \frac{c_{12}}{i\mu\omega} \qquad c_{34} = \frac{c_{11}}{\sigma_o} \qquad c_{43} = \frac{c_{22}}{i\mu\omega} \qquad c_{44} = \frac{c_{21}}{\sigma_o}$$

and $\left| a_n(R) \right| = x_1 x_2 = -x_1^2 / k_o^2$.

The desired result $[d_{ij}] = a_n(a)\, a_n^{-1}(R)$ will involve products of Hankel functions at $\underline{a}$ and $\underline{R}$; but these can all be expressed in terms of $H_{n+\frac{1}{2}}(k_o a)$ and $H_{n-\frac{1}{2}}(k_o a)$ using the following expansions:

$$H_{n+\frac{1}{2}}(k_o R) = H_{n+\frac{1}{2}}(k_o a)\left[1 - \frac{h}{a}\left(n+\frac{1}{2}\right) \right] + k_o h\, H_{n-\frac{1}{2}}(k_o a) \qquad \text{A.3.1}$$

and $$H_{n-\frac{1}{2}}(k_o R) = -k_o h\, H_{n+\frac{1}{2}}(k_o a) + H_{n-\frac{1}{2}}(k_o a)\left[1 + \frac{h}{a}\left(n-\frac{1}{2}\right) \right] \qquad \text{A.3.2}$$

which result from using the first two terms of the Taylor series for the Hankel function at R in terms of one at $\underline{a}$.

The required solution is

$$a_n(a)\, a_n^{-1}(R) = [a_{ij}]\, [c_{ij}] / x_1 x_2$$

and in the approximation that $\frac{h}{a} \sim \frac{h}{R} \ll 1$ [which also means that $W(k_o R) \sim W(k_o a)$]

$$a_n(a)\, a_n^{-1}(R) = \begin{vmatrix} 1 & -i\mu\omega h(1-n(n+1)/k_o^2 a^2) & 0 & 0 \\ k_o^2 h / i\mu\omega & 1 & 0 & 0 \\ 0 & 0 & 1 & i\mu\omega h \\ 0 & 0 & -\frac{k_o^2 h}{i\mu\omega}(1-n(n+1)/k_o^2 a^2) & 1 \end{vmatrix}$$

The preceeding matrix is denoted as equation A.3.3. This matrix applies to the air layer between the source and the ionosphere. For the extremely thin layer between the earth's surface and the source $a_n(r_n)\, a_n^{-1}(r_{n+1}) = I$, the unit matrix, since there will be no change in an ELF wave over such a short interval.

Determination of a single 4x4 matrix to express $a_n(r_n)\, a_n^{-1}(r_{n+1})$ in the ionosphere is somewhat more lengthy in algebra since there are no zeros in the a_n's. Referring to the section on the wave solutions in anisotropic media for spherical coordinates,

$$a_n(r_n) = \begin{array}{cccc} \text{(out)} & \text{(in)} & \text{(out)} & \text{(in)} \\ k_1 x_n \exp(ik_1 r_n) & -k_1 x_n \exp(-ik_1 r_n) & k_3 y_n \exp(ik_3 r_n) & -k_3 y_n \exp(-ik_3 r_n) \\ z_n \exp(ik_1 r_n) & z_n \exp(-ik_1 r_n) & z_n \exp(ik_3 r_n) & z_n \exp(-ik_3 r_n) \\ ik_1 x_n \exp(ik_1 r_n) & -ik_1 x_n \exp(-ik_1 r_n) & -ik_3 y_n \exp(ik_3 r_n) & ik_3 y_n \exp(-ik_3 r_n) \\ -iz_n \exp(ik_1 r_n) & -iz_n \exp(-ik_1 r_n) & iz_n \exp(ik_3 r_n) & iz_n \exp(-ik_3 r_n) \end{array}$$

where $k_1^2 = k_\perp^2 + ik_x^2$, $k_3^2 = k_\perp^2 - ik_x^2$, and

$$x_n = \frac{i\sigma_{11}}{r_n(\sigma_\perp + i\sigma_x)}, \qquad y_n = \frac{i\sigma_{11}}{r_n(\sigma_\perp - i\sigma_x)}, \qquad z_n = \frac{-\sigma_{11}}{r_n}$$

and the σ's pertain to the nth layer from r_n to r_{n+1}.

The determinant $\left|a_n(r_{n+1})\right| = 16 k_1 k_3 x_{n+1} y_{n+1} z_{n+1} z_{n+1}$.

The inverse matrix $a_n^{-1}(r_{n+1})$ is given as follows:

$$a_n^{-1}(r_{n+1}) = \begin{vmatrix} \frac{\exp(-ik_1 r_{n+1})}{4k_1 x_{n+1}} & \frac{\exp(-ik_1 r_{n+1})}{4z_{n+1}} & \frac{-i\exp(-ik_1 r_{n+1})}{4k_1 x_{n+1}} & \frac{i\exp(-ik_1 r_{n+1})}{4z_{n+1}} \\ \frac{-\exp(ik_1 r_{n+1})}{4k_1 x_{n+1}} & \frac{\exp(ik_1 r_{n+1})}{4z_{n+1}} & \frac{i\exp(ik_1 r_{n+1})}{4k_1 x_{n+1}} & \frac{i\exp(ik_1 r_{n+1})}{4z_{n+1}} \\ \frac{\exp(-ik_3 r_{n+1})}{4k_3 y_{n+1}} & \frac{\exp(-ik_3 r_{n+1})}{4z_{n+1}} & \frac{i\exp(-ik_3 r_{n+1})}{4k_3 y_{n+1}} & \frac{-i\exp(-ik_3 r_{n+1})}{4z_{n+1}} \\ \frac{-\exp(ik_3 r_{n+1})}{4k_3 y_{n+1}} & \frac{\exp(ik_3 r_{n+1})}{4z_{n+1}} & \frac{-i\exp(ik_3 r_{n+1})}{4k_3 y_{n+1}} & \frac{-i\exp(ik_3 r_{n+1})}{4z_{n+1}} \end{vmatrix}$$

Finally, if we let $h_n = r_{n+1} - r_n$, then $a_n(r_n)\, a_n^{-1}(r_{n+1}) = [\, c_{ij}\,]$ where

$$c_{11} = \frac{1}{2}\left[\cos(k_1 h_n) + \cos(k_3 h_n)\right] r_{n+1}/r_n = c_{22} = c_{33} = c_{44}$$

$$c_{12} = \frac{-i}{2z_{n+1}}\left[k_1 x_n \sin(k_1 h_n) + k_3 y_n \sin(k_3 h_n)\right] = -c_{34}$$

$$c_{13} = \frac{i}{2}\left[-\cos(k_1 h_n) + \cos(k_3 h_n)\right] r_{n+1}/r_n = -c_{31} = -c_{24} = c_{42}$$

$$c_{14} = \frac{1}{2z_{n+1}}\left[k_1 x_n \sin(k_1 h_n) - k_3 y_n \sin(k_3 h_n)\right] = c_{32}$$

$$c_{21} = \frac{-iz_n}{2}\left[\frac{1}{k_1 x_{n+1}} \sin(k_1 h_n) + \frac{1}{k_3 y_{n+1}} \sin(k_3 h_n)\right] = -c_{43}$$

$$c_{23} = \frac{-z_n}{2}\left[\frac{1}{k_1 x_{n+1}} \sin(k_1 h_n) - \frac{1}{k_3 y_{n+1}} \sin(k_3 h_n)\right] = c_{41}$$

BIOGRAPHICAL NOTE

W. B. Thompson was born and attended school in Meriden, Connecticut. He received a B. S. and M. S. in Geology and Geophysics at M.I.T. in 1958. After one year at California Institute of Technology, he returned to continue graduate study at M.I.T.

He has held the position of Research Assistant in the Department of Geology and Geophysics and in the M.I.T. Research Laboratory of Electronics during the course of this dissertation.

BIBLIOGRAPHY

Aikin, A. C., 1962, Charged Particle Reactions of Importance in the Ionosphere, Goddard Space Flight Center Publication X-615-62-132.

Akasofu, S., 1956, Science Reports of the Tohoku University, Fifth Series, Geophysics, Vol. 8, No. 1, pp.24-39.

Balser, M. and C. A. Wagner, 1960, Observations of the Earth-Ionosphere Cavity Resonances, Nature, Vol. 188, No. 4751, pp. 638-641.

Balser, M. and C. A. Wagner, 1961, Diurnal Power Variations of the Earth-Ionosphere Cavity Modes and their Relationship to World-Wide Thunderstorm Activity, M. I. T., Lincoln Laboratory Report 35G-0005.

Balser, M. and C. A. Wagner, 1962, On Frequency Variations of the Earth-Ionosphere Cavity Modes, J. Geophys. Res., Vol. 67, No. 10, pp. 4081-4083.

Bourdeau, R. E., 1962, Space Flight Studies of the Ionosphere, Goddard Space Flight Center Publication X-615-62-204.

Bourdeau, R. E., E. C. Whipple, Jr., and J. F. Clark, 1959, Analytic and Experimental Conductivity Between the Stratosphere and the Ionosphere, J. Geophys. Res., Vol. 64, No. 10, pp. 1367-1370.

Chapman, S., 1956, The Electrical Conductivity of the Ionosphere--A Review, Nuovo Cimento (Supplement), pp. 1385-1412., Vol. 4, Ser. X

Fejer, J. A., 1960, Hydromagnetic Wave Propagation in the Ionosphere, J. Atm. and Terr. Phys., Vol. 18, pp. 135-146.

Francis, W. E. and R. Karplus, 1960, Hydromagnetic Waves in the Ionosphere, J. Geophys. Res., Vol. 65, No. 11, pp. 3593-3600.

Galejs, J., 1961, Terrestrial Extremely Low-Frequency Noise Spectrum in the Presence of Exponential Ionospheric Conductivity Profiles, J. Geophys. Res., Vol. 66, No. 9, pp. 2787-2792.

Galejs, J., 1962, A Further Note on Terrestrial Extremely Low-Frequency Propagation in the Presence of an Isotropic Ionosphere with an Exponential Conductivity--Height Profile, J. Geophys. Res., Vol. 67, No. 7, pp. 2715-2728.

Handbook of Geophysics, 1960, U. S. Air Force, ARDC, AFCRC, The MacMillan Co., New York.

Huxley, 1953, Experimental Study of Motions of Slow Electrons in Air with Applications to the Ionosphere, Proc. Royal Soc., 218, p. 507.

Ionospheric Radio Propagation, 1948, N. B. S. Circular 462.

Johnson, C. Y., E. B. Meadows, and J. C. Holmes, 1958, Ion Composition of the Arctic Ionsophere, J. Geophys. Res., Vol. 63, pp. 443-4.

Johnson, F. S., 1961, Satellite Environment Handbook, Stanford University Press.

Madden, T. R., 1961, An Analysis of the Earth-Ionosphere Electromagnetic Resonance, Class Note for M. I. T. Course 12.88, Spring Term.

Mitra, S. K., 1952, The Upper Atmosphere, The Asiatic Society, Calcutta.

Moler, W. F., 1960, VLF Propagation Effects of a D-Region Layer Produced by Cosmic Rays, J. Geophys. Res., Vol. 65, No. 5, pp. 1459-1468.

Nicolet, M., and A. C. Aikin, 1960, Formation of the D Region of the Ionosphere, J. Geophys. Res., Vol. 65, No. 5, pp. 1469-1482.

Poeverlein, H., 1959, Transparency of the Ionosphere and Possible Noise Signals from High Altitudes at Extremely Low Frequencies, AGARDograph, 42, Paris, France.

Raemer, H. R., 1961, On the Extremely Low Frequency Spectrum of Earth-Ionosphere Cavity Response to Electric Storms, J. Geophys. Res., Vol. 66, No. 5, pp. 1580-1583.

Ratcliffe, J. A., 1959, The Magneto-Ionic Theory and Its Applications to the Ionosphere, Cambridge University Press.

Sagalyn, R. C., M. Smiddy, and J. Wisnia, 1963, Measurement and Interpretation of Ion Density Distributions in the Daytime F Region, J. Geophys. Res., Vol. 68, No. 1, pp. 199-212.

Schumann, W. O., 1952, Uber die Ausbreitung sehr langer elektrischer Wellen und der Blitzentladung um die Erde, Z. angew. Phys., Vol. 4, pp. 474-480.

Schumann, W. O., 1957, Elektrische Eigenschwingungen des Hohlraumes Erde-Luft-Ionosphare, Z. angew. Phys., Vol. 9, pp. 373-378.

Stratton, J. A., 1941, Electromagnetic Theory, McGraw-Hill, New York.

Taylor, H. A., Jr., and H. C. Brinton, 1961, Atmospheric Ion Composition Above Wallops Island, Virginia, J. Geophys. Res., Vol. 66, No. 8, pp. 2587-2588.

Watanabe, K. and H. E. Hinteregger, 1962, Photoionization Rates in the E and F Regions, J. Geophys. Res., Vol. 67, No. 3, pp. 999-1005.